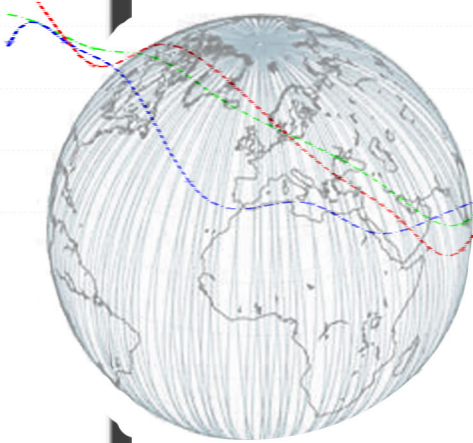
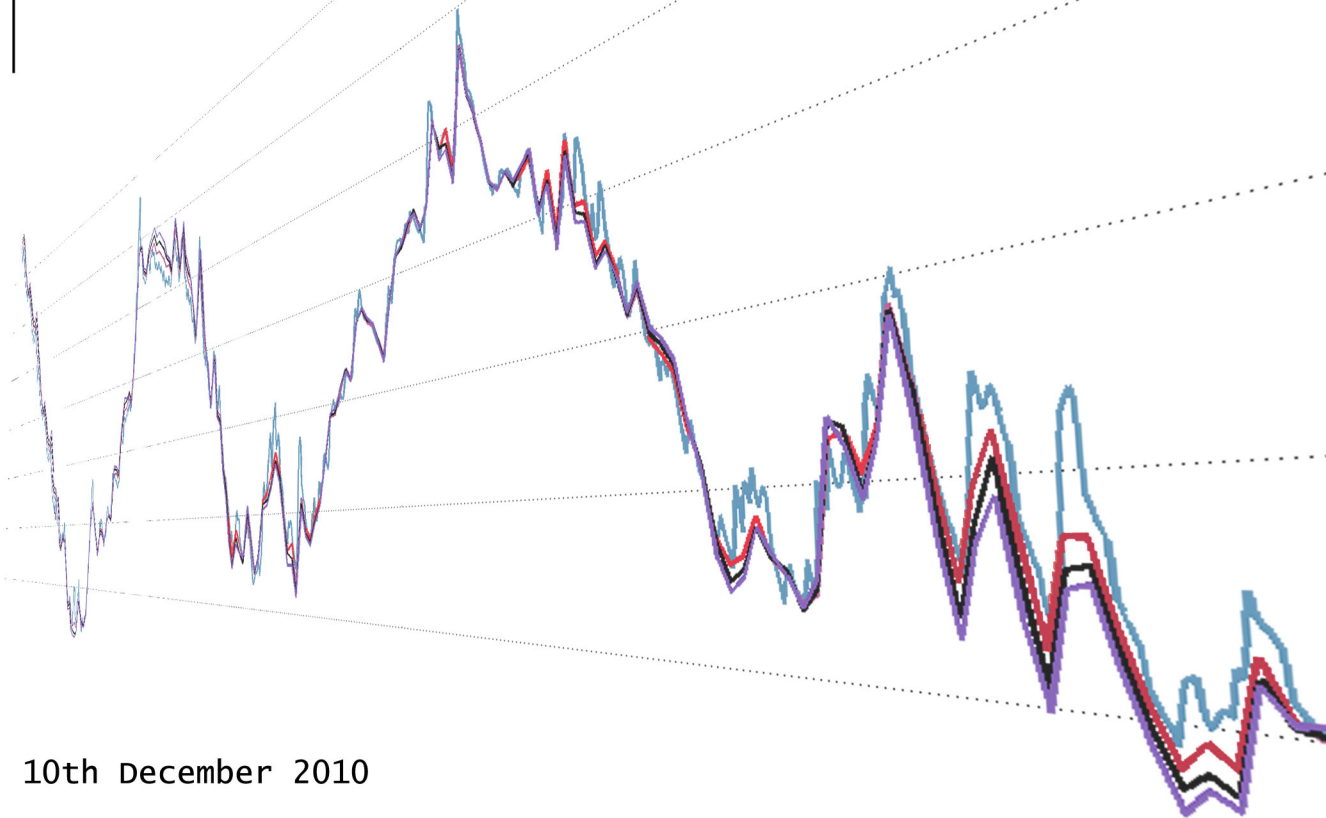


Efstratios Tzompanopoulos



Assimilating GRACE Terrestrial Water Storage observations into a conceptual hydrological model



10th December 2010

Assimilating GRACE Terrestrial Water
Storage observations into a conceptual
hydrological model

Efstratios Tsompanopoulos

10th December 2010

Title:

Assimilating GRACE Terrestrial Water Storage observations into a conceptual hydrological model

By:

Efstratios Tsompanopoulos

Student Number:1541749

Msc Geomatics

Graduation professor:

Prof. dr. ir. Nick C. van de Giesen

Water Resources Management, Faculty of Civil Engineering and Geosciences,
TU Delft.

Daily supervisor:

Dr. ir. Susan C. Steele-Dunne

Water Resources Management, Faculty of Civil Engineering and Geosciences,
TU Delft.

Committee members:

Dr. Brian C. Gunter

Physical and Space Geodesy, Faculty of Aerospace Engineering, TU Delft.

Dr. Albrecht Weerts

Deltares

Date: 10th December 2010

Abstract

Based on satellite observations of Earth's time variable gravity field from the Gravity Recovery and Climate Experiment (GRACE), it is possible to derive variations in terrestrial water storage. Tiny variations of gravity from monthly into a decade time scales are mainly due to redistributions of water mass inside the surface fluid envelopes of our planet (Ramillien et al., 2008). This allows us to derive variations in TWS (Terrestrial Water Storage) from satellite observations of the gravity field.

Firstly, the Ensemble Kalman filter (EnKF) and the Ensemble Kalman smoother (EnKS) have been applied to assimilate the GRACE TWS variation data into the HBV-96 model, a conceptual rainfall-runoff model over the Rhine river basin. Based on prior work on this field, in this thesis it was intended from the very beginning the improvement of methods used, starting from the study period, which was extended from February 1st 2003 to December 26st 2006.

Afterwards, newer versions of TWS variation estimates were inferred from three sets of GRACE solutions, one from DEOS TU Delft, and another from CSR - University of Texas. A third dataset named as RBF, based on radial basis function was also included. All of the solutions use different filtering methods which yield different estimates.

The following step was to change the state vector and how it is updated. In this way a more realistic method for the individual stores of the Terrestrial Water Stores was used.

Finally the Ensemble Moving Batch Smoother have been applied to assimilate the GRACE data into the HBV-96 model. This new assimilation smoother uses observations beyond the estimation time, which are also useful in the estimation.

Preface

First and foremost, I would like to thank my daily thesis supervisor, Dr. Susan Steele-Dunne, for her tireless support, education and most of all patience in teaching and supervising me. I found this interesting thesis topic through Prof. Nick van de Giesen who is my thesis professor and I would like to thank him also. This master thesis wouldn't have happened without the support of my other two committee members: Dr. Brian Gunter who had provided me with the GRACE data and Dr. Albrecht Weerts from Deltares who had provided me the hydrological model and data, and to them I extend my gratitude for all their help throughout this research.

This thesis and my studies in general wouldn't have been possible without my parents, whom support was tremendous and I would like to thank them from the bottoms of my heart. Also, I would like to thank my friend and partner Lia, for all the support and patience she had during my master studies. Last, but not least, I would like to give my warm thanks to all of my friends, and especially the 'Fockstraat' company whom support and help lead me through those two years in Delft.

Efstratios Tsompanopoulos

Delft, December 2010.

CONTENTS

List of Figures	xi
1 Introduction	1
1.1 Motivation	1
1.2 Research objectives	2
1.3 Thesis Outline	2
2 Background	5
2.1 Terrestrial Water Storage	5
2.2 Hydrological model	6
2.2.1 HBV-96	7
2.3 GRACE	9
2.4 GRACE Data-sets	12
2.4.1 DEOS DMT-1	13
2.4.2 CSR RL04	13
2.4.3 RBF	14
2.5 GRACE - Hydrological Model	15
2.6 Study Area	16

3	Data Assimilation	19
3.1	Introduction	19
3.2	What is Data Assimilation?	20
3.3	Ensemble Kalman Filter	21
3.4	Ensemble Kalman Smoother	23
3.5	Ensemble Moving Batch Smoother	25
4	Model Uncertainty	29
4.1	Introduction	29
4.2	Perturbing Parameters	29
4.2.1	Parameter Model Maps	30
4.2.2	Forcing Data Maps	30
4.3	Ensemble Open Loop	32
5	Initial Simulations	35
5.1	Extending the simulation period	35
5.1.1	Introduction	35
5.1.2	Implementation	35
5.1.3	Results	39
5.2	Debugging	41
5.3	GRACE Algorithms Comparison	44
5.3.1	Introduction	44
5.3.2	Implementation	44
5.3.3	Results - Discussion	44
6	Definition of state vector	49
6.1	State Vector Disaggregation Change	49
6.1.1	Introduction	49
6.1.2	Implementation	49
6.1.3	Results - Discussion	51
6.2	State Vector Change	53
6.2.1	Introduction	53

6.2.2	Implementation	53
6.2.3	Results - Discussion	55
7	Ensemble Moving Batch Smoother	61
7.1	Ensemble Moving Batch Smoother	61
7.1.1	Implementation	61
7.1.2	Results - Discussion	64
7.2	EnMB with increased maximum limitations	67
7.2.1	Introduction	67
7.2.2	Implementation	68
7.2.3	Results - Discussion	68
8	Conclusions	73
	Bibliography	77

LIST OF FIGURES

2.1	Conceptualization of the Water Cycle (www.usgcrp.gov/) . . .	6
2.2	Structure of the HBV model (parameters in bold capitals)(after Seibert (1999))	8
2.3	GRACE satellite mission: the flight configuration and ground support (after eosps0.gsfc.nasa.gov/)	10
2.4	Spatial coverage of GRACE groundtracks, indicating the trade-off between spatial and temporal resolution (after Schmidt et al. (2008))	11
2.5	Maps of GRACE TWS for April 2005 for the three datasets. The datasets depict the differences to a reference month. Beware of the different color-bars (the mean on those plots is not added).	14
2.6	The location of Rhine river Basin in Europe (after Terink et al. (2010))	16
2.7	The Rhine river Basin and its subcatchments (after Widiastuti (2009))	17
3.1	Variational data assimilation method. The prior model state is given a better initial condition that leads to an update model state that is closer to the observations (Widiastuti (2009), after (Drecourt, 2004))	21

3.2	Sequential data assimilation method. When an observation is available, the model state is updated to a value closer to the observation that is used to make the next prediction (Widiastuti (2009), after (Drecourt, 2004))	21
3.3	Illustration of the update procedure used in the EnKF (Evensen, 2007)	24
3.4	Illustration of the update procedure used in the EnKS (Evensen, 2007)	24
3.5	Conceptual diagram of EnMB smoother algorithm. An estimate of the state is required at every time step, while observations are available at every fourth time step (after Dunne and Entekhabi (2005))	26
4.1	Catchment averaged ensemble mean Terrestrial Water Storage of Ensemble Open Loop (upper plot). Catchment averaged ensemble standard deviation of TWS for Ensemble Open Loop (lower plot)	32
4.2	TWS individual stores of the Ensemble Open Loop (ensemble mean and standard deviation)	33
5.1	Flow diagram of the GRACE Ensemble Kalman Filter and Ensemble Kalman Smoother. SM is for soil moisture, UZ is for upper zone and LZ is for lower zone (after Widiastuti (2009)).	36
5.2	Averaged catchment ensemble mean TWS of Ensemble Kalman Filter compared with the GRACE DMT observation dataset and ensemble mean TWS of Ensemble Open Loop (upper plot). Averaged catchment ensemble standard deviation of TWS for Ensemble Kalman Filter compared with EnsOL (lower plot).	37
5.3	EnKF and EnKS ensemble mean TWS of the averaged catchment and ensemble standard deviation of TWS. The observation dataset used is GRACE DMT. The three different EnKS updates (5, 10, and 15 days before the update day) denoted as lag1,2,3	38
5.4	Zoom in at the first eight months of the EnKF and EnKS simulation of the previous plot (Standard Deviation of the averaged catchment)	39
5.5	Bug-Debug comparison of Ensemble Kalman Filter (in mm) .	40

5.6	Debugged EnKF and EnKS ensemble mean TWS of the averaged catchment. The observation dataset used is GRACE DMT. The three different EnKS updates (5 days step) denoted as lag1,2,3	41
5.7	Debugged EnKF and EnKS ensemble standard deviation of the TWS for the averaged catchment. The observation dataset used is GRACE DMT. The three different EnKS updates (5 days step) denoted as lag1,2,3	42
5.8	Individual stores (Upper zone, Lower zone and Soil moisture) of the averaged catchment after de-bugging compared with Ensemble Open Loop individual stores (in mm)	42
5.9	Averaged catchment mean TWS (in mm) for: Ensemble Open Loop, Ensemble Kalman Filter, Ensemble Kalman Smoother with three different steps denoted as lag1,2,3. All compared to GRACE observation (DMT algorithm).	43
5.10	Comparison of the three datasets of GRACE Observations, DTM, RBF and CSR (TWS averaged catchment in mm)	45
5.11	Comparison of the different GRACE algorithms. Ensemble Kalman Filter was used for the mean of the TWS averaged catchment in mm	45
5.12	Comparison of the different GRACE algorithms. The standard deviation of the of the TWS averaged catchment in mm (Ensemble Kalman Filter)	46
5.13	The three different algorithms compared for the 18-May-2003, simulated using the Ensemble Kalman Filter (Catchment in mm)	46
5.14	The three different algorithms (simulated using the Ensemble Kalman Filter) compared with the Ensemble Open Loop (TWS averaged catchment in mm)	47
5.15	Comparison of the individual stores for the three different algorithms (simulated using the Ensemble Kalman Filter)(ensemble mean for averaged catchment per store in mm)	48
6.1	Schematic view of the state vector change. In prior simulations the updated TWS was disaggregated into SM-LZ-UZ, while afterwards the sequence was changed into SM-UZ-LZ.	50

6.2	Ensemble mean TWS value of the averaged catchment for both of the simulations. In prior simulations the updated TWS was disaggregated into SM-LZ-UZ, while afterwards the sequence was changed into SM-UZ-LZ	52
6.3	Averaged Catchment ensemble standard deviation of TWS for the simulations. In prior simulations the updated TWS was disaggregated into SM-LZ-UZ, while afterwards the sequence was changed into SM-UZ-LZ	52
6.4	Comparison of the individual stores for both of the simulations. In prior simulations the updated TWS was disaggregated into SM-LZ-UZ (old), while afterwards the sequence was changed into SM-UZ-LZ (new)	53
6.5	Flow diagram of the Ensemble Kalman Filter and Ensemble Kalman Smoother simulation with the new state update vector. SM is for soil moisture, UZ is for upper zone and LZ is for lower zone.	54
6.6	Ensemble Kalman Filter and Ensemble Kalman Smoother assimilating the DMT observation data where the layers are updated individually. Ensemble mean TWS and ensemble Standard deviation of TWS for the averaged catchment	56
6.7	Individual stores update compared with the Ensemble open loop. SM is for soil moisture, UZ is for upper zone and LZ is for lower zone.	57
6.8	Individual stores comparison between the EnKF simulation with (New SV) and without (Old SV) individual update of the layers. SM is for soil moisture, UZ is for upper zone and LZ is for lower zone. Also, SV is for state vector.	57
6.9	Terrestrial Water Storage comparison between the Ensemble Kalman Filter simulation with individual update in state vector (new) and without individual update (old), with the Ensemble Open Loop and DMT observation	58
7.1	Flow diagram of the Ensemble Moving Batch Smoother	62
7.2	Conceptual diagram of the Ensemble Moving Batch Smoother used in this master thesis	63
7.3	Ensemble mean TWS of the averaged catchment for Ensemble Moving Batch and Ensemble Open Loop (DMT algorithm was used)	64

7.4	Averaged catchment ensemble standard deviation of TWS for the Ensemble Moving Batch and the Ensemble Kalman Filter (DMT algorithm was used)	65
7.5	Comparison of individual stores for the Ensemble Moving Batch compared with the Ensemble Open Loop. SM is for soil moisture, UZ is for upper zone and LZ is for lower zone.	65
7.6	Individual stores for the Ensemble Moving Batch compared with the Ensemble Kalman Filter. SM is for soil moisture, UZ is for upper zone and LZ is for lower zone.	66
7.7	Comparison of the Soil Moisture layer for the Ensemble Moving Batch with the Ensemble Open Loop. The Ensemble Moving Batch is plotted with and without the final step of the EnsOL (in mm)	67
7.8	Averaged catchment ensemble mean TWS value for the Ensemble Moving Batch simulations, Ensemble Open Loop and GRACE observation. The different EnMB plots represent the old and new limitations of the Lower and Upper zone (in mm).	69
7.9	Averaged catchment ensemble standard deviation of the TWS for the Ensemble Moving Batch simulations. The different EnMB plots represent the old and new limitations of the Lower and Upper zone (in mm). The framed parts depict the 'M' pattern.	69
7.10	Individual stores for the different Ensemble Moving Batch simulations, with and without increased limitation for lower and upper zone. SM is for soil moisture, UZ is for upper zone and LZ is for lower zone (in mm)	70
7.11	Individual stores for the different Ensemble Moving Batch simulations, with and without increased limitation for lower and upper zone. SM is for soil moisture, UZ+LZ is the accumulated lower and upper zone (in mm)	71
7.12	Comparison of the Soil Moisture layer for the Ensemble Moving Batch with the Ensemble Open Loop. The Ensemble Moving Batch is plotted with and without the final step of the EnsOL (in mm)	71

CHAPTER 1

INTRODUCTION

1.1 Motivation

Estimates of terrestrial water storage can have important political and economic implications, as they are critical for understanding and predicting climate change, weather, agriculture productivity, flooding, and other natural hazards (Tapley et al., 2004).

As it will be explained in the next chapters, it is difficult to determine directly the Terrestrial Water Storage on continental scales. Research (Rammillien et al., 2008; Rodell et al., 2007; Schmidt et al., 2006; Werth et al., 2009; Widiastuti, 2009) has shown that GRACE satellite gravimetry offers a very interesting alternative remote sensing technique to measure changes in total water storage (ice, snow, surface waters, soil moisture, groundwater) over continental areas, representing a new source of information for hydrologists and global hydrological modelers.

The outcome of my research in assimilating GRACE terrestrial water storage data into the HBV-96, should be to improve even more the methodology developed by Widiastuti (2009). The qualitative impact should be to extract better quality results after the simulation; more accurate and closer to the expected outcomes. The final evaluation of my work will be based on how are those changes on the algorithms or in the previous procedures, will affect the result and if the new procedures will be included into the method in total.

1.2 Research objectives

Already from Widiastuti (2009) case study, the results are very promising. The Ensemble Kalman Filter and Smoother were successfully implemented; they were used to assimilate GRACE observations to the HBV model.

The first thing I am going to improve in the implementation period is to extend the period of simulation. In this way, I can answer my basic questions: what leads to an update? Do the initial conditions create the ensemble spread or the winter which creates some kind of seasonality? The implementation period will be separated in four steps:

- Algorithm development (Time extension from one year to three years and change of update vector)
- Test several different GRACE observations algorithms
- Test a new state vector, where the individual stores of the Terrestrial Water Storage will be updated individually
- Test a new ensemble smoother (Ensemble Moving Batch Smoother) for data assimilation

All those implementation steps will be done by acquiring the GRACE data from Dr. Brian C. Gunter (Physical and Space Geodesy, Faculty of Aerospace Engineering, TU Delft), and the Hydrological model and data from Dr. Albrecht Weerts (Deltares).

1.3 Thesis Outline

The scope of this master thesis is to use Kalman filters, to assimilate satellite observations into a hydrological model. In the 2nd chapter, all the background information for the proper understanding and use of this master thesis is introduced. In the beginning of the chapter the Terrestrial Water Storage is defined. Then, general information for hydrological modelling are given and also all details for the model used in this master thesis. Afterwards GRACE mission is explained, as well as the three datasets which are used in the simulations. Also, some cases where hydrological modelling was combined with GRACE data are analyzed. Finally, some basic information for the case study area is presented.

In the next chapter there is an analysis of data assimilation and also for the specific Kalman Filters and Smoothers used in this master thesis. In chapter number four, the model uncertainty is analyzed and the results of the initial perturbation and Ensemble Open Loop are shown.

In the 5th chapter the initial simulations are presented. In this chapter the first two research questions are answered. The 6th chapter is dealing with the third research objective which has to do with the state vector definition. In the 7th chapter the Ensemble Moving Batch is analyzed, applied and the results are commented.

Finally, the conclusions chapter should give an overall view of the progress which was made through this thesis, some comments about the final results and suggestions for future work.

CHAPTER 2

BACKGROUND

This Chapter provides background information for this master thesis. In the first part the terrestrial water storage and its importance to water management is analyzed and also how it can be estimated by means of hydrological modelling. The hydrological model which is used in this master thesis is also described.

In the next part there is description of GRACE satellite mission and gravity field observations. Also the different algorithms of processing the initial GRACE data are explained.

Afterwards those two different sections are combined to explain how information from both hydrological modelling and GRACE observation can be combined to provide a better estimate of terrestrial water storage. Finally details are given for the study area of this master thesis.

2.1 Terrestrial Water Storage

Terrestrial water storage (TWS) can be defined as all forms of water stored above and underneath the surface of the Earth (Syed et al., 2008), which can include water in vegetation surfaces, snow, ice, soil water, groundwater, surface water in rivers, lakes, wetlands and man-made reservoirs.

For a hydrologist there are two major problems to deal with; firstly to quantify the amount of water in the different hydrological cycle phases and seasonally to evaluate the rate of transfer of water between the cycle phases

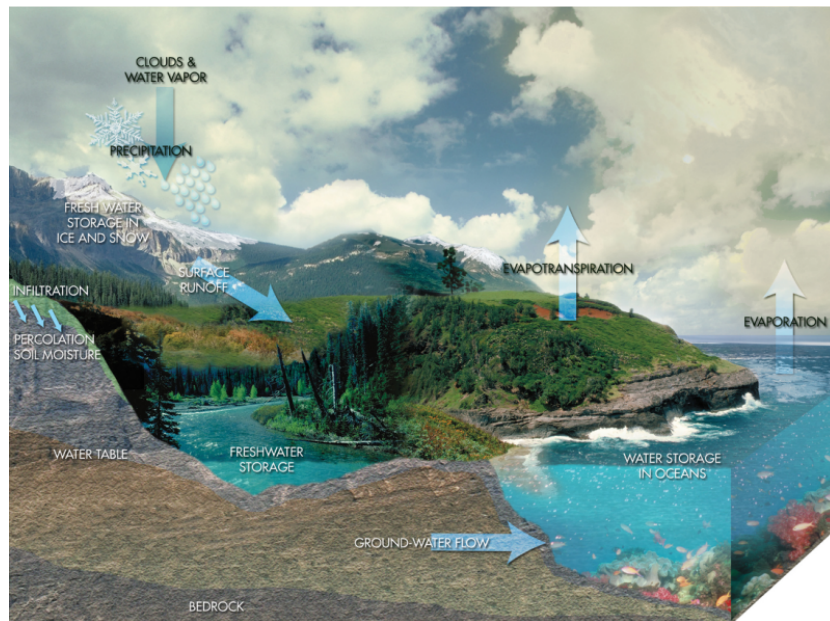


Figure 2.1: *Conceptualization of the Water Cycle (www.usgcrp.gov/)*

(Shaw, 1983). Individual soil moisture or groundwater measurements provide only local estimates of water storage. Thus temporal and spatial variations of water storage are presently not known with sufficient accuracy for large areas (Schmidt et al., 2006).

Estimation of terrestrial water storage is possible by using hydrological models. There is a large number of hydrological models available, and they vary in terms of process description, temporal resolution, spatial resolution, and the detail in process representation. The following section explains the different types of hydrological model.

2.2 Hydrological model

As mentioned in the previous section, the TWS estimation is really difficult in large-scale monitoring systems. But as the latest decades the technology had developed, also in the field of Hydrology there were some changes. High speed processors and the large storage capability of modern personal computer, provide to the Hydrology scientists the appropriate tools to develop more efficient and effective models.

A rainfall-runoff model describes the rainfall-runoff relations of a rainfall catchment area, drainage basin or watershed. There are two really important

parameters which affects this kind of models. Firstly those models are very much dependent on the time scale being considered. For short timescales their relationship cannot be easily defined but in a long duration period the connection becomes much simpler. The other important parameter is the size of area to be considered. Small and homogenous areas could be treated easily while large drainage basins with national or international scales, differences in catchment effects are smoothed out giving relatively simply rainfall-runoff relationships (Shaw, 1983).

Already from 1960, the Hydrologists started to investigate the rainfall - runoff relations of a rainfall catchment area (Dooge, 1959; Nash, 1960). Nash (1960) presented his concept of the unit hydrograph as the end product of a series of successive linear storages in the watershed. And it was also Dooge (1959) who used linear storages interspersed with time delays. The 1960's brought intensive studies of this outflow hydrography as a nonlinear function (Linsley, 1967).

An hydrological transport model (or simply Hydrological model) could be defined as a mathematical model used to simulate river or stream flow and calculate water quality parameters. According to Shaw (1983) Hydrological models can be divided into two groups. Firstly there are the deterministic models (also known as Physically-based models), which seek to simulate the physical processes in the catchment involved in the transformation of rainfall to streamflow. Secondly there are the stochastic models which describe the hydrological time series of the input variables such as rainfall, evapotranspiration or streamflow involving distributions in probability (Shaw, 1983).

Finally, conceptual modelling should be mentioned. Hydrologists use conceptual modelling to simplify the complex processes which take place in the hydrological cycle. This kind of modelling divides the whole hydrology possesses of a drainage basin, into reservoirs for which water budgets are kept (Shaw, 1983).

2.2.1 HBV-96

In the previous section there is a discussion about what is an Hydrological model and the different types of hydrological models were analyzed. Also, there is a discussion about the characterization rainfall-runoff of a model and how a conceptual model could simplify the complex processes of hydrology. In this section a brief description of the hydrology model used in this master thesis, known as HBV-96 (Hydrologiska Byrans Vattenbalansavdelning model of 1996) is given.

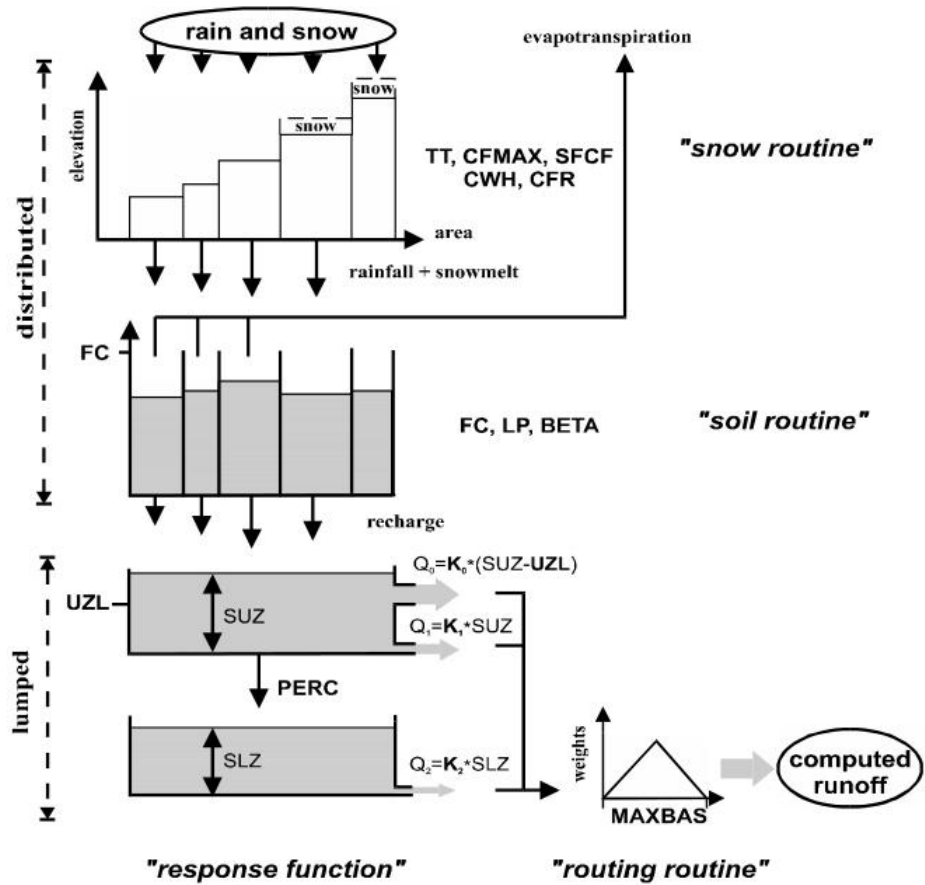


Figure 2.2: Structure of the HBV model (parameters in bold capitals)(after Seibert (1999))

The HBV-Model is a semi-distributed conceptual rainfall-runoff model, which simulates snow accumulation, snow melt, actual evapotranspiration, soil moisture storage, groundwater depth and runoff (www.smhi.se/en). The HBV-96 model is a newer version of the SMHI model (Swedish Meteorological and Hydrological Institute) created by Bergstrom (1976). Lindstrom et al. (1997) created the final HBV-96 model after a comprehensive reevaluation.

As shown in Figure 2.2, the model consists of different routines, where snow-melt is computed by a degree-day method. Groundwater recharge and actual evaporation are functions of actual water storage in a soil box and runoff formation is represented by three linear reservoir equations and channel routing is simulated by a triangular weighting function (Seibert, 1999).

We already have defined HBV model as semi-distributed. This means

that a basin may be separated into a number of subbasins and that each one of these is distributed according to elevation and vegetation. The HBV model has gradually been developed into a semi-distributed model (Lindstrom et al., 1997).

The hydrological model which is used in this case is a calibrated version of HBV-96 model, by Deltares research institute, for the Rhine river-basin Weerts (2010). The model used in this thesis was programmed in PCRaster environment (Utrecht University).

The input data required by the HBV-96 model are precipitation, air temperature, and evapotranspiration of a daily timestep. The available data for this thesis are from January 1st 2001 until December 31st 2005, and the grid size is 1 km (Weerts, 2009). All prior work (mostly MatLab code) was developed and provided by Widiastuti (2009).

2.3 GRACE

The launch of the Gravity Recovery and Climate Experiment (GRACE) twin satellite mission in March 2002 has provided the first space based data-set for large scale TWS estimates. Although primarily aimed at accurately mapping time variations in Earth's gravity field at 30 day intervals, GRACE has shown remarkable prospects for inferring water mass changes over the globe (Tapley et al., 2004). The GRACE satellite mission's goal is to map the Earth's time-varying gravity field with a temporal resolution of 1 month or better and a spatial resolution of about 400 km.

The GRACE mission is a first realization of the so-called satellite-to-satellite tracking concept in the low-low mode dating back to the fundamental paper by Wolff (1969). Wolff (1969) in his article "Direct measurements of the Earth's Gravitational Potential Using a satellite pair", said that it is possible to measure variations of intensity of the earth's gravity field by orbiting two geometrically identical satellites spaced about 200 kilometers apart and equipped to measure their relative velocity. The basic idea is to trace the spatio-temporal gravity field with an increased sensitivity by means of micrometer-precise inter-satellite range and range-rate observations of two co-planar orbiting satellites. As the two satellites move along their orbit, separated by a mean inter-satellite distance of approximately 220 km, the relative motion of the spacecraft, visible as continuous variations in the measured range and range-rate, respectively, is proportional to the integrated differences of the gravity accelerations felt by each satellite at its individual position (Schmidt et al., 2008).

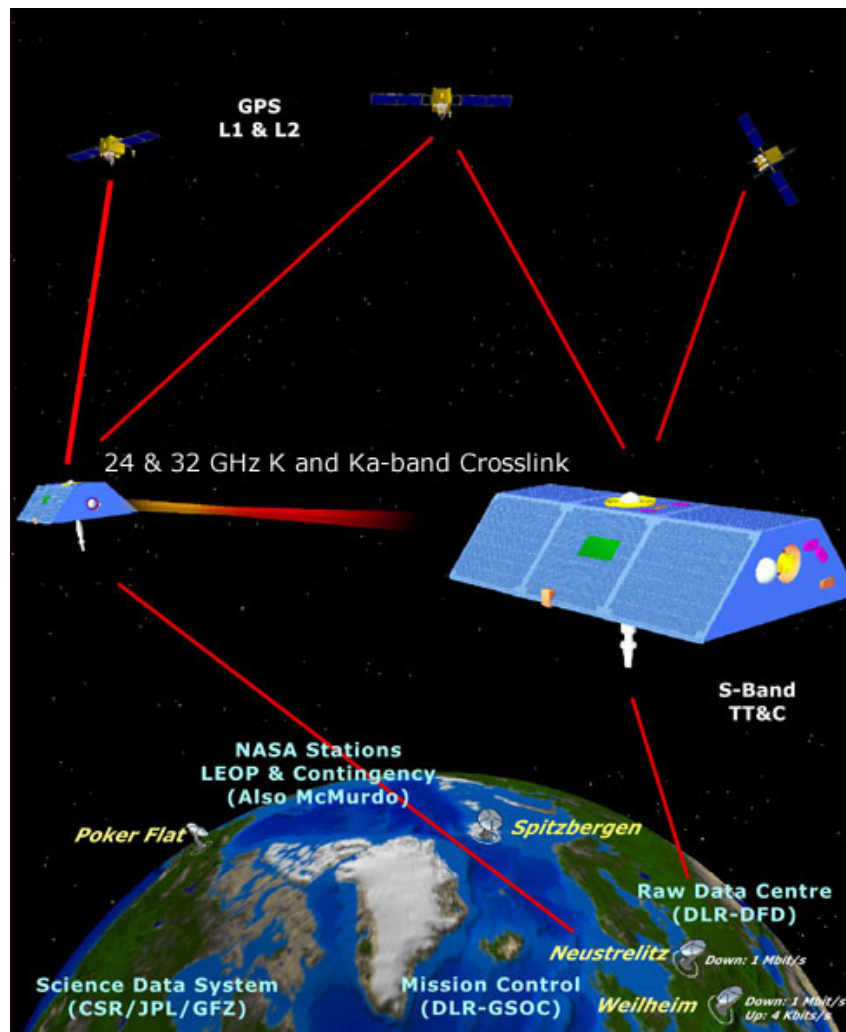


Figure 2.3: *GRACE satellite mission: the flight configuration and ground support (after eospos.gsfc.nasa.gov/)*

Some basic characteristics are given below:

- The mission was launched on 17 March 2002 and it has recently been agreed to extend the experiment to the end of its on-orbit life, which expected in 2015 (www.nasa.gov)
- The system's initial altitude was 500 km (the orbit altitude is not kept fixed and decreases due to air drag with an average rate of about 2.7 km/year). This low altitude was selected to allow for a detection of the gravity signals in the inter-satellite data well above the micron level, as Wolff (1969) suggested

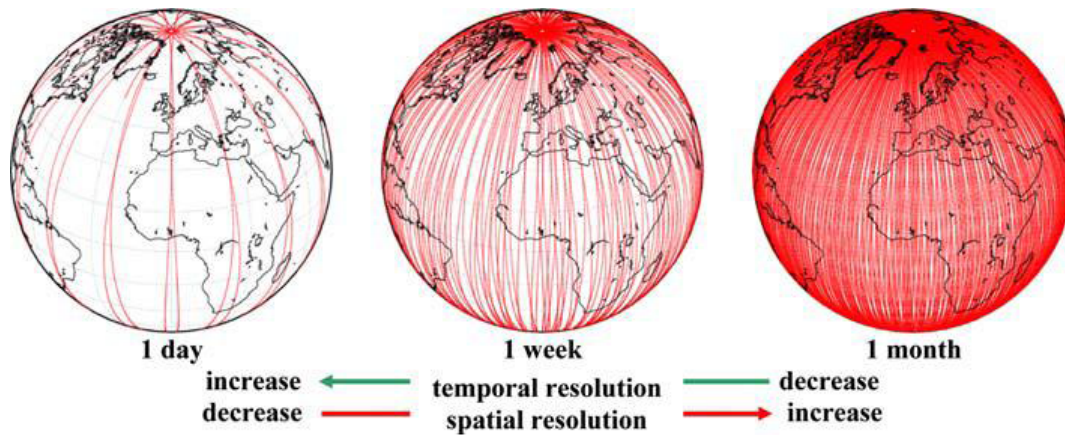


Figure 2.4: *Spatial coverage of GRACE groundtracks, indicating the trade-off between spatial and temporal resolution (after Schmidt et al. (2008))*

- To yield a global coverage, an almost polar inclination has been selected of 89.5°
- Absolute positioning of the two spacecraft and the inter-satellite observations, is provided by a space-proved multi-channel, two-frequency GPS receiver onboard each GRACE satellite, known as GPS-SST (satellite to satellite)
- K-band range and range-rate satellite-to-satellite tracking between the two GRACE satellites, known as KBR-SST (satellite to satellite)

Monthly gravity field estimates made by the twin Gravity Recovery and Climate Experiment (GRACE) satellites have a geoid height accuracy of 2-3 millimeters at a spatial resolution as small as 400 kilometers. The trade-off between spatial and temporal resolution is illustrated in Figure 2.4.

Observations of seasonal variations in Earth's gravity field place important constraints on models of global mass variability and temporal exchange among the land, ocean, and atmosphere. This is particularly important for subsystems that might otherwise be extremely difficult to detect and monitor. Terrestrial water variations are the largest omitted phenomena and are thus the dominant unmodeled signal that should be evident in the monthly gravity estimates (Tapley et al., 2004).

2.4 GRACE Data-sets

Monthly GRACE gravity field models are very noisy. When computing the monthly mean water storage variation over a target area, the noise is partially reduced, but still is unacceptable high. Therefore, some additional spatial smoothing is required prior to the computation of mean monthly mass variations over a target area (Jekeli, 1981; Klees et al., 2006; Kusche, 2007).

The standard method is to apply Gaussian Smoothing with radius of 300-500 Km (Jekeli, 1981). More recent works tend to apply probabilistic decorrelation methods in the post-processing of GRACE solutions, usually in conjunction with an additional smoothing. The idea behind the decorrelation is to identify and remove error correlation in the sets of spherical harmonic coefficients (i.e. between different coefficients).

Official global gravity field models are computed from GRACE data by the Center of Space Research (CSR) of the University of Texas at Austin; by the GeoForschungsZentrum Potsdam in collaboration with Groupe de Recherche de Geodesie Spatiale (GFZ/GRGS) and by the Jet Propulsion Laboratory (JPL) of the California Institute of Technology. In addition, alternative solutions are computed by several other research groups like the Delft Institute of Earth Observation and Space Systems (DEOS) at Delft University of Technology; the Centre National d'Etudes Spatiales (CNES). In this thesis there are used three types of datasets, the DEOS DMT-1 solution, the CSR-RL04 solution and the RBF solution (radial basis functions (RBFs) as parametrization). Details about the GRACE solutions used for simulation are described in the following subsections.

The idea behind the GRACE gravity field solution, is to follow four basic steps:

- Firstly, to obtain the monthly sets of inter-satellite differences. Those differences in most cases of datasets are range-rates, but alternatively could be to use directly to use range measurements and also derived range-accelerations
- Monthly mass variations (unconstrained) in equivalent water height
- Monthly mass variations (optimally filtered). This is the step where the basic modelling for each of the databases takes place
- Linear trends (filtered). This final step is where the filter, the additional smoothing is applied to the datasets

All the data used and presented in this thesis are in the Gauss Krueger Zone 3 coordinate system. The Gauss Krueger Zone 3 (Pulkovo 1942(83)) is a German coordinate system, and it was used because the majority of the study area lies on Germany.

2.4.1 DEOS DMT-1

The DEOS solutions are a series of monthly estimates of the Earth's gravity field variation with respect to the static gravity field EIGEN-GL04C (Liu, 2008). The N-Body Perturbations were done according to DE405 planetary ephemerides. There were used IERS 2003 conventions for the Solid Earth (pole) tides. For the Ocean tides FES2004 model is used. Finally for general relativity effects were used, IERS 2003 conventions (DEOS, 2009).

Computation of the monthly solutions involved the following basic steps: First the computation of purely dynamic orbits of GRACE satellites. Secondly the derivation of residual range combinations and afterwards the computation of monthly solutions and corresponding covariance matrices. Fourth and final step is the post-processing of the monthly solutions. The first three steps are described in detail in Liu (2008). A detailed description of the posteriori filtering of monthly solutions, which is the most essential part of the final step, is given in Klees et al. (2008b).

The series of monthly solutions is post-processed by applying statically optimal Wiener-type filters based on full signal and noise covariance matrices (Klees et al., 2008b). Details on the procedure of building these filters are given by Liu et al. (2010).

The data which were used was from February of 2003 until February of 2009. Both of datasets there were provided by the DEOS department (Gunter, 2010).

2.4.2 CSR RL04

The CSR solutions are produced by the Center of Space Research (CSR) at University of Austin. The monthly solutions issued by CSR have several versions. The Release 04 (RL04) products are used in this thesis for the simulations, analysis and comparison with the other solutions. The monthly solutions contain fully normalized spherical harmonic coefficients up to degree and order 60 (Liu, 2008). More details of the RL04 model computation processing can be found in (Bettadpur, 2007).

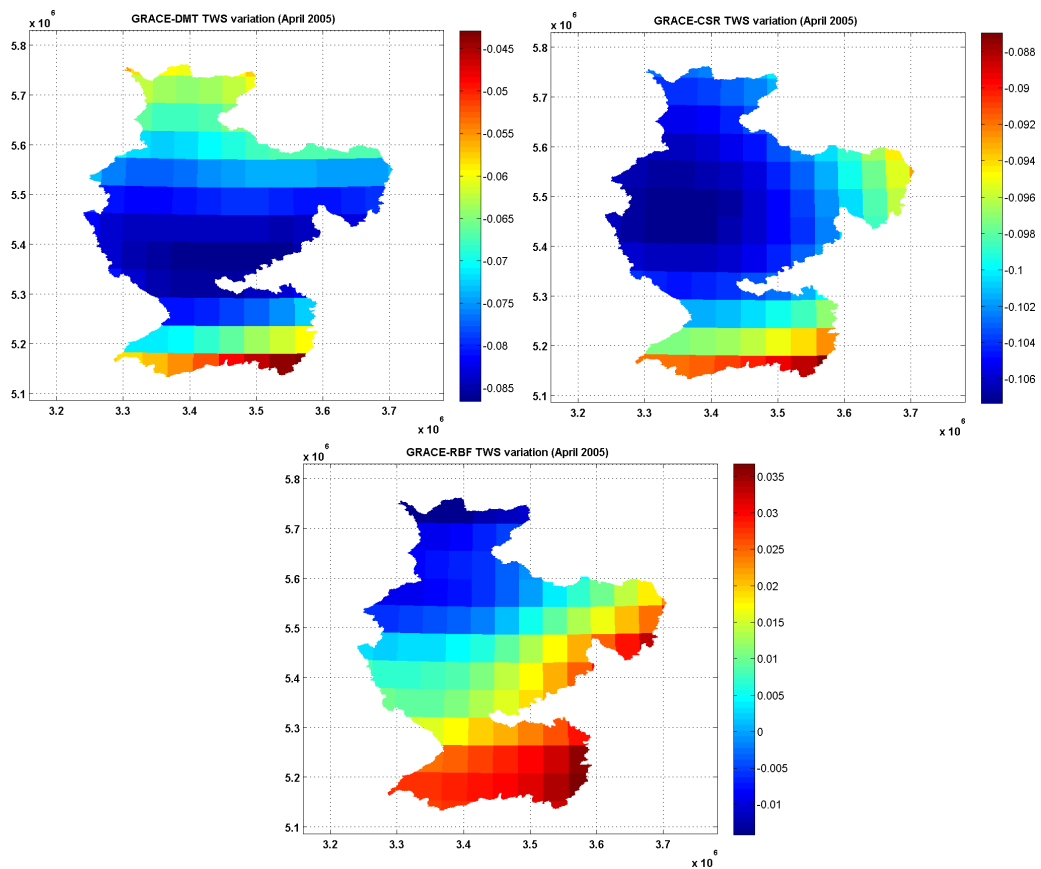


Figure 2.5: Maps of GRACE TWS for April 2005 for the three datasets. The datasets depict the differences to a reference month. Beware of the different color-bars (the mean on those plots is not added).

The data were processed in the Delft Institute of Earth Observation and Space Systems (DEOS) of TU Delft. The datasets were 'destriped' using the Swenson and Wahr (2006) approach. It was applied a 400 km halfwidth Gaussian smoothing in the spherical harmonics and then converted to grids of equivalent water height, using the methodology presented by Wahr et al. (1998). Then the DS400 was applied as explained in depth from Swenson et al. (2008).

2.4.3 RBF

Radial basis functions are radial-symmetric functions which are localising in space, i.e. most of their energy is confined to a local area. They have either global or local support (Wittwer, 2009).

There are several analysis centers such as DEOS, the Institute of Theoretical Geodesy (ITG) at the University of Bonn, the Goddard Space Flight Center (GSFC), and others, that compute solutions for several areas of interest using spherical radial basis functions (SRBFs) or single layer densities (mascons) as an alternative to the spherical harmonic representation of surface mass change. Those solutions are attractive for two main reasons firstly they require only a limited set of GRACE data to be processed and a relatively small number of basis functions, and secondly they are expected to exploit the resolution of the GRACE observations better than the spherical harmonic basis functions (Klees et al., 2008a). More details on how the RBF dataset is created are given by Wittwer (2009). The datasets in this thesis provided by the DEOS department (Gunter, 2010).

Figure of all three datasets, interpolated for the whole time span which they are going to be used is provided in section 5.3.3 (Figure 5.10).

2.5 GRACE - Hydrological Model

The launch of the GRACE satellite mission in 2002, has provided a new source of information for hydrologists and global hydrological modelers (Ramillien et al., 2008). In the next paragraphs a summary of the researches done using GRACE data and a Hydrological model is given.

In Ramillien et al. (2008), there is an analysis of several areas of Hydrology, affected by the ability of GRACE to detect hydrological signals with sufficient accuracy. Pre-launch assessments (Rodell and Famiglietti, 1999, 2001, 2002) as well as several post-launch studies (Ramillien et al., 2004; Wahr et al., 2004) have clearly demonstrated the capability of GRACE to monitor water storage variations like.

In the same article (Ramillien et al., 2008), there is a clear reference in the fact that a global network for monitoring continental water storage will likely not appear in the near-future, while the spatial resolution of GRACE data has been steadily improving thanks to advances in both processing of the instrument data and post-processing of the gravity field solutions using linear filtering.

When Rodell and Famiglietti (1999) compared some modelled datasets of TWS to expected GRACE instrument errors, they found that the detectable limit of spatial scales to water storage changes would be $200,000 \text{ km}^2$ or greater, and at the same time for monthly or longer timescales, and with monthly accuracies of roughly 1.5 cm .

In terms of accuracy, studies have demonstrated the possibilities of such a satellite system to detect and monitor spatial redistribution of TWS versus time, at the precision of only tens of millimeters of equivalent-water height. The accuracy of the results still depends upon the low-pass filtering method used, and so the level of noise in the GRACE data (Ramillien et al., 2008).

Also, Klees et al. (2008a) describes that the typical accuracy of current GRACE solution for river basins above 1 million km^2 is 20 mm equivalent water height. In this master thesis and for all the GRACE datasets which are used for the simulations, an accuracy of 20 mm will be used, following the typical accuracy of GRACE.

2.6 Study Area

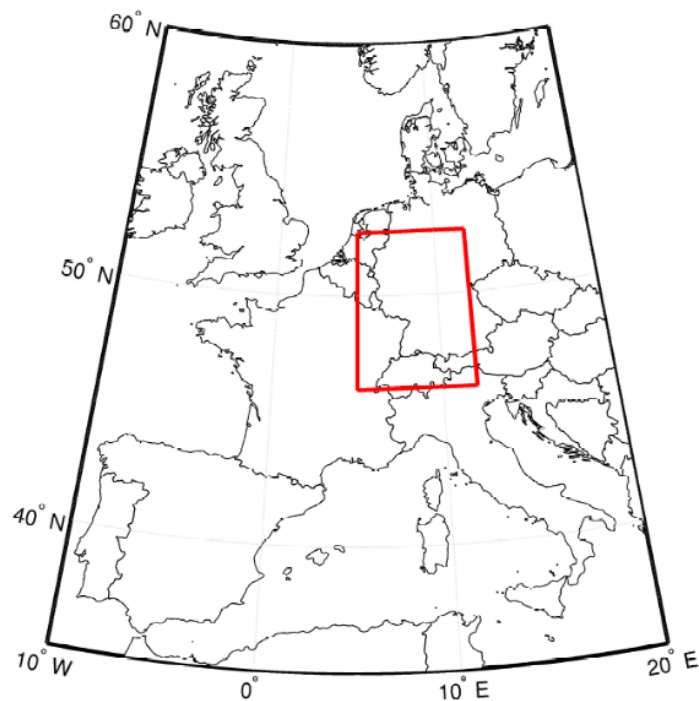


Figure 2.6: *The location of Rhine river Basin in Europe (after Terink et al. (2010))*

The study area of this Master Thesis is the Rhine river basin. The Rhine is one of the longest and most important rivers in Europe, at 1320 km, with an average discharge of $2200 m^3/s$. The river basin has a population of 50

million. The total drainage area is 185000 Km^2 , although in this case study, the lowland region is excluded, leaving an area of 160000 Km^2 . (en.wikipedia.org/wiki/Rhine; www.grid.unep.ch)

Etymologically Rhine's name has its roots from the Gaulish "Renos", which means literally "that which flows". The spelling with -h- seems to be borrowed from the Greek form of the name, Rhenos (www.etymonline.com/).

The Rhine river is the major river in western Europe, and as we can see from Figures 2.6 and 2.7, its basin covers portions of seven European countries: Switzerland, Liechtenstein, Austria, Germany, Germany, France and Netherlands. It is also important that in the Rhine river basin there are 18 Ramsar Sites protected.

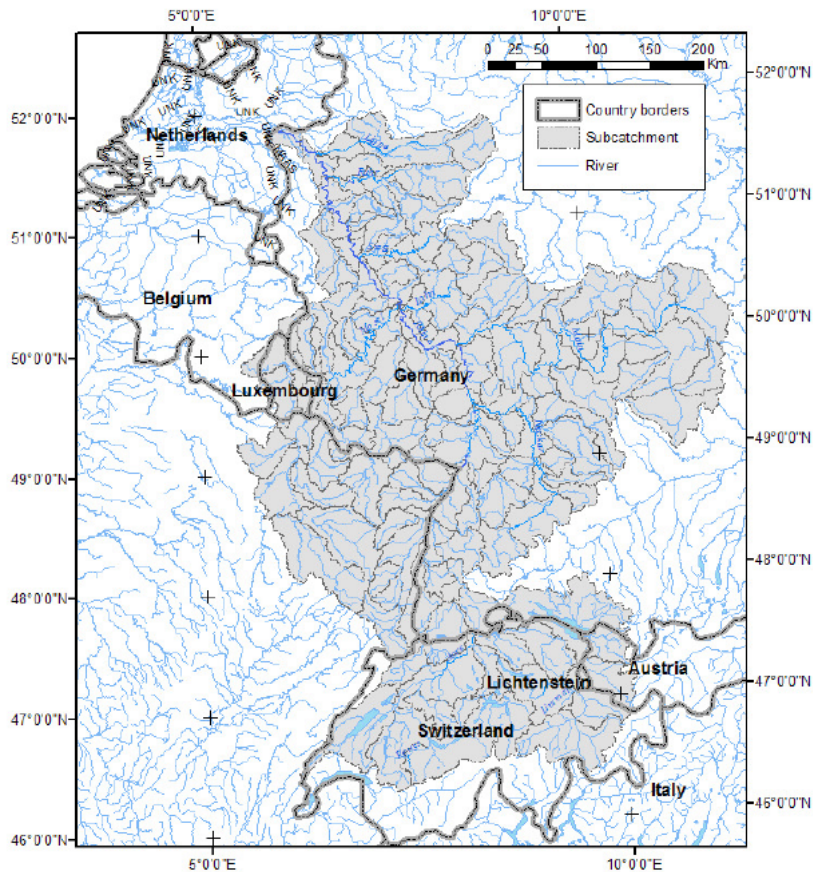


Figure 2.7: *The Rhine river Basin and its subcatchments (after Widiastuti (2009))*

The basins climate is determined by its location in a zone of temperate climatic conditions with frequent weather changes. There is precipitation all

the year round, varying from 700 to 1,200 *mm*. The annual mean temperature is around 9 C. The impacts resulting from Climate Change scenarios on the discharge regime of the Rhine, based on simulations using the Rhineflow model, are:

- The discharge regime of the Rhine (and especially in the Swiss part of the catchment) is expected to shift away from a snowfall-snowmelt controlled regime to one that is much more rainfall controlled.
- This change in discharge regime, combined with the increased winter precipitation, will result in substantially increased winter discharges (up to 40 percent increase)
- The change in discharge regime, combined with the increased temperature will result in a decrease in summer discharge of about 15 percent (www.unesco-ihp.org/; www.waterandclimate.org/)

3.1 Introduction

In order to assimilate the GRACE data into the hydrological model the method that it will be used is the Ensemble Kalman Filter and the Ensemble Kalman Smoother. Previous research (Margulis et al. (2002), Reichle et al. (2002), Dunne and Entekhabi (2006), Widiastuti (2009), Drecourt (2004)), has shown that applying Ensemble Kalman methods to assimilate remote sensing data into hydrology data had great results. In particular Reichle et al. (2002) mention in their research that EnKF (Ensemble Kalman Filter) is an attractive option for land applications. That is because (i) its sequential structure is convenient for processing remotely sensed measurements in real time, (ii) it provides information on the accuracy of its estimates, (iii) it is relatively easy to implement even if the model and measurement equations include thresholds and other nonlinearities, and (iv) it is able to account for a wide range of possible model errors.

Data assimilation can be loosely defined as the combination of the complementary information from reliable observations and dynamic model into an optimal estimate of an unknown true state.

The EnKS (Ensemble Kalman Smoother), was firstly introduced by Evensen and van Leeuwen (2000). The EnKS can be regarded as an extension of the EnKF (Ensemble Kalman Filter). The EnKF was first introduced by Evensen (1994) and it gained popularity because of its simple conceptual formulation and relative ease of implementation. The EnKS, as described in

Evensen and van Leeuwen (2000), updates the ensemble at prior times every time new measurements are available. It allows for a sequential processing of the measurements in time. Thus, every time a new set of measurements becomes available, the ensemble at the current and all prior times can be updated (Evensen, 2003). The Ensemble Moving Batch Smoother was initially introduced by Dunne and Entekhabi (2005). It is a simple extension of the EnKF in which the states are distributed in time and updated in a 'batch'.

In section 3.2 the term data assimilation is explained. In the following sections the the different methods which are used (Ensemble Kalman Filter, Ensemble Kalman Smoother and Ensemble Moving Batch Smoother) are explained.

3.2 What is Data Assimilation?

Data assimilation is a mathematical method in which observations of the current (and possibly, past), are combined with results of a numerical model. This combination takes place in every analysis step of the analysis cycle in which the model proceeds. At the analysis step, data assimilation tries to balance the uncertainty in the data and in the forecast. The model is then advanced in time and its result becomes the forecast in the next analysis cycle (Bouttier and Courtier, 1999).

Why use Data Assimilation rather than modeling alone? Always in a model we have to deal with some kind of structural errors which could be some weak assumptions in the basis of the model due to insufficient knowledge of the working field, or there could be simplifications, or approximations. Imperfect model inputs could compromise the result and there are always in modelling some uncertain model parameters (Evensen, 2007).

Drecourt (2004), in his PhD thesis, mentions that the main strength of data assimilation is the *ability to extract the optimal amount of information out of the observations*. Provided that the errors on the observations and the model are estimated properly, data assimilation gives the optimal estimate of the state of the system .

There are two basic approaches to data assimilation: sequential assimilation, that only considers observation made in the past until the analysis step, which is the case of real-time assimilation systems, and non-sequential, or variational assimilation, where observation from the future can be used, for instance in a reanalysis exercise. Sequential methods include the classic Kalman Filter, the Extended Kalman Filter, the Ensemble Kalman Filter

and the Ensemble Kalman Smoother, while variational methods are 3D-Var or 4D-Var (Bouttier and Courtier, 1999).

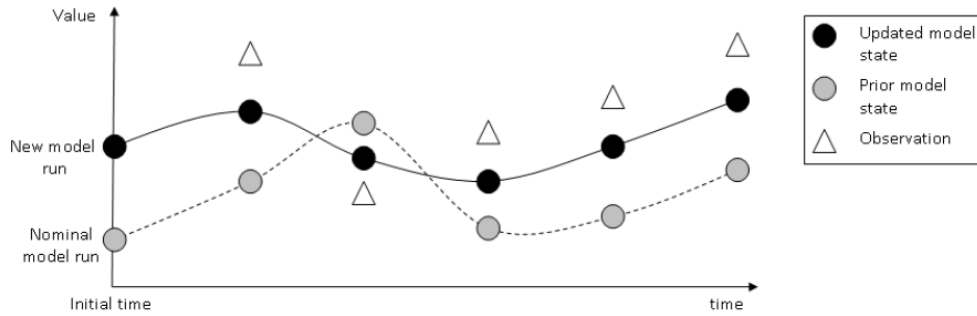


Figure 3.1: Variational data assimilation method. The prior model state is given a better initial condition that leads to an update model state that is closer to the observations (Widiastuti (2009), after (Drecoart, 2004))

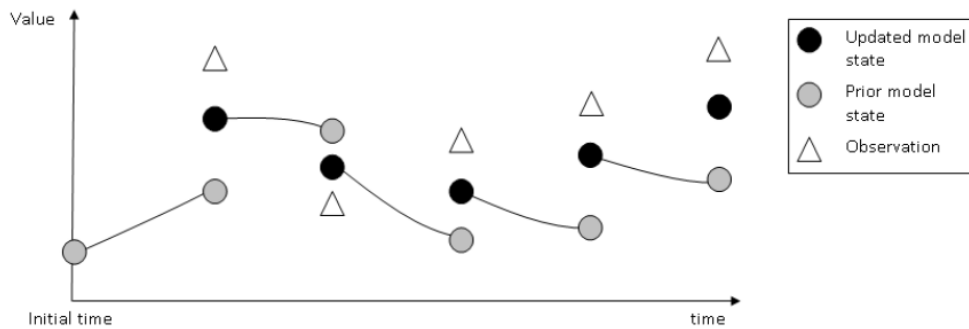


Figure 3.2: Sequential data assimilation method. When an observation is available, the model state is updated to a value closer to the observation that is used to make the next prediction (Widiastuti (2009), after (Drecoart, 2004))

Both the Ensemble Kalman Filter and Ensemble Kalman Smoother (EnKS) use a Monte Carlo or ensemble representation for the pdfs (Probability density function), an ensemble integration using stochastic models to model the time evolution of the pdfs (Evensen, 2007).

3.3 Ensemble Kalman Filter

The Kalman filter is the most well-known data assimilation technique. It has quite simple implementation and it has also gained this popularity due to its

relative robustness to the misspecification of the error sources (Madsen and Canizares, 1999).

The reason for not using KF (Kalman filter) or EKF (Ensemble Kalman Filter) is that both of them propagate error information with a dynamic equation for the state error covariance matrix. However, the integration of this equation is not computationally feasible for large scale environmental systems. Is the same reason that made Evensen (1994) to use an ensemble of model trajectories from which the necessary error covariances are estimated at the time of an update. The technique has since become known as the Ensemble Kalman filter (Reichle et al., 2002). The method uses the nonlinear model to propagate the ensemble states. Some of the linearizations that make the EKF prone to failure are thereby avoided.

The Kalman filter is in essence a Best Linear Unbiased Predictor (BLUP). This means that Kalman Filter is optimal in situations when we have a linear model. Also it is a minimum variance estimate, i.e. given a model forecast and an observation, it provides the estimate that minimizes the estimation variance (Drecourt, 2004).

The objective of the Ensemble Kalman Filter is to estimate the value of the states of the system stored in the state vector y . The state y is propagated forward in time using the model, in this case the hydrological model. At each update time t , a vector of observations (z) becomes available. A non linear operator M relates the true state to the measured variable.

$$z(t) = M[y(t)] + e(t) \quad (3.1)$$

where the uncertainty in the observation is given in the vector e , which is assumed to be zero mean with covariance matrix R_e . For a given vector of measurements at time t , an ensemble of perturbed observation is generated:

$$z_j(t) = z(t) + \epsilon_j(t) \quad (3.2)$$

where j refers to the j_{th} ensemble member. If the ensemble of perturbations is gathered into the matrix $\gamma = (\epsilon_1, \epsilon_2, \dots, \epsilon_1 N)$, the measurement covariance can be written as

$$R_\epsilon = \frac{\gamma\gamma^T}{N-1} \quad (3.3)$$

The analysis or update (a) is obtained by updating each replicate individually:

$$y_j^a(t) = y_j(t) + K(t)(z_j(t) - M[y_j(t)]) \quad (3.4)$$

where $K(t)$ is the Kalman gain matrix:

$$K(t) = C_{YM}(C_M + R_\epsilon)^{-1} \quad (3.5)$$

C_{YM} is the forecast cross covariance between the state $y(t)$ and the measurement predictions $M[y(t)]$. C_M is the forecast error covariance of the measurement predictions. If the states, perturbed observations and predicted measurements are gathered into the matrices Y , Z and M respectively, then the terms of the Kalman gain matrix can be written as

$$C_{YM} = \frac{1}{N-1} Y' M'^T \quad (3.6)$$

$$C_M = \frac{1}{N-1} M' M'^T \quad (3.7)$$

Equation 3.4 can therefore be expressed as:

$$Y^a(t) = Y(t) + Y'(t) M'^T(t) \{ M'(t) M'^T(t) + \gamma \gamma^T \}^{-1} (Z(t) - M(t)) \quad (3.8)$$

In Figure 3.3, the EnKF is explained schematically. The horizontal axis is time and the measurements are indicated at regular intervals. The vertical axis indicates the number of updates with measurements. The blue arrows represent the forward ensemble integration, the red arrows are the introduction of measurements, while the green arrows is the EnKF update algorithm. Thus, the blue arrows indicate the EnKF solution as a function of time, which is updated every time measurements are available.

3.4 Ensemble Kalman Smoother

The Ensemble Kalman Smoother was firstly introduced by Evensen and van Leeuwen (2000) and it is based on ensemble statistics. It bears a strong resemblance with the ensemble Kalman filter. The difference is that every time a new dataset is available during the forward integration, an analysis is computed for all previous times up to this time. Thus, the first guess for the

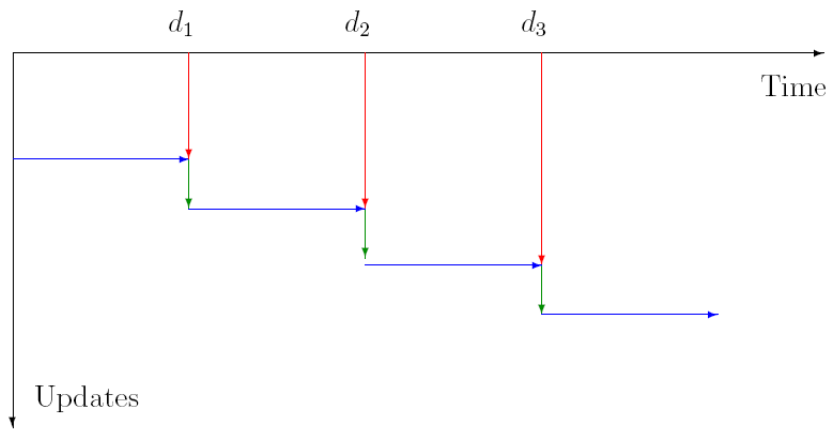


Figure 3.3: *Illustration of the update procedure used in the EnKF (Evensen, 2007)*

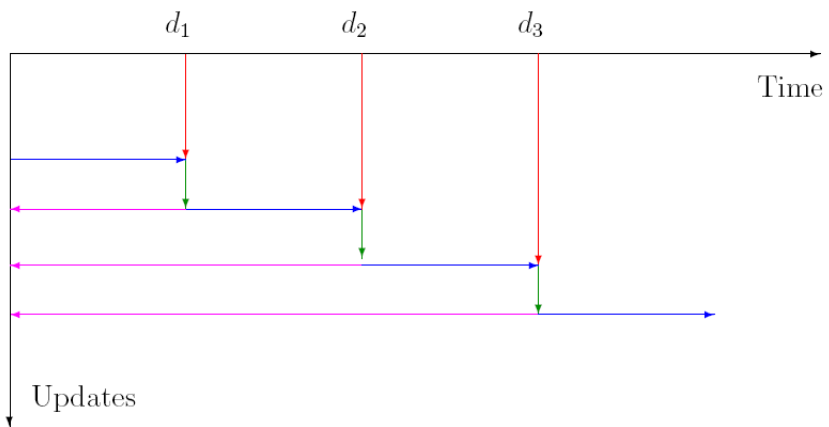


Figure 3.4: *Illustration of the update procedure used in the EnKS (Evensen, 2007)*

smoother is the ensemble Kalman filter solution, and the smoother estimate provides an improvement of this, as one would expect a smoother to do.

The Ensemble Kalman Smoother (EnKS) is a straight forward extension of the EnKF. As the EnKF uses the ensemble covariances in space to spread the information from the measurements, the EnKS uses the ensemble covariances in space and time to spread the information also backward in time Evensen (2007).

In the EnKS, the information from the observation at update time t is used to update the state estimate at the update time and also at previous times t' using:

$$Y^a(t') = Y(t') + Y'(t')M'^T(t)\{M'(t)M'^T(t) + \gamma\gamma^T\}^{-1}(Z(t) - M(t)) \quad (3.9)$$

The EnKS is a sequential algorithm, requiring only forward model runs, and no additional model runs beyond those required by the EnKF. The EnKF solution is used as the first estimate of the EnKS. Each update with a subsequent set of observations results in a change in ensemble mean and a reduction in ensemble variance. So, the EnKS estimates should always be at least as good as the EnKF. As observations further into the future are used, the improvements become negligible, indicating that they are beyond the decorrelation time (Evensen, 2003).

In equation 3.9, if the terms pertaining to time (t) are grouped together in $B(t)$, then we have:

$$Y^a(t') = Y(t') + Y'(t')B(t) \quad (3.10)$$

which $B(t)$ is common with equation 3.8 of the EnKF. So, at an update time t , the matrix $B(t)$ is computed to update the current state in the EnKF. The same matrix could be used in EnKS. A computationally expensive calculation is therefore avoided.

Figure 3.4, explains the EnKS schematically. The horizontal axis is time and the measurements are indicated at regular intervals. The vertical axis indicates the number of updates with measurements. The blue arrows represent the forward ensemble integration, the red arrows are the introduction of measurements, while the green arrows denote updates. Thus, the blue arrows indicate the EnKF solution as a function of time, which is updated every time measurements are available. The magenta arrows are the updates for the EnKS, which goes backward in time, and which is computed following the EnKF update every time measurements are available.

3.5 Ensemble Moving Batch Smoother

In the development and application of EnKF techniques there have been several recent changes. Dunne and Entekhabi (2005) argued that soil moisture estimation is a reanalysis-type problem as observations beyond the estimation time are also useful in the estimation. However, the EnKF uses only observations prior to the estimation time to update the current state. To overcome this problem they developed an Ensemble Moving Batch (EnMB)

smoother in which all observations within a prescribed window were used to update all of the soil moisture states in a batch. The EnMB uses the EnKF equations but has a state vector that is distributed in time. It was shown that smoothing improved the estimates of soil moisture.

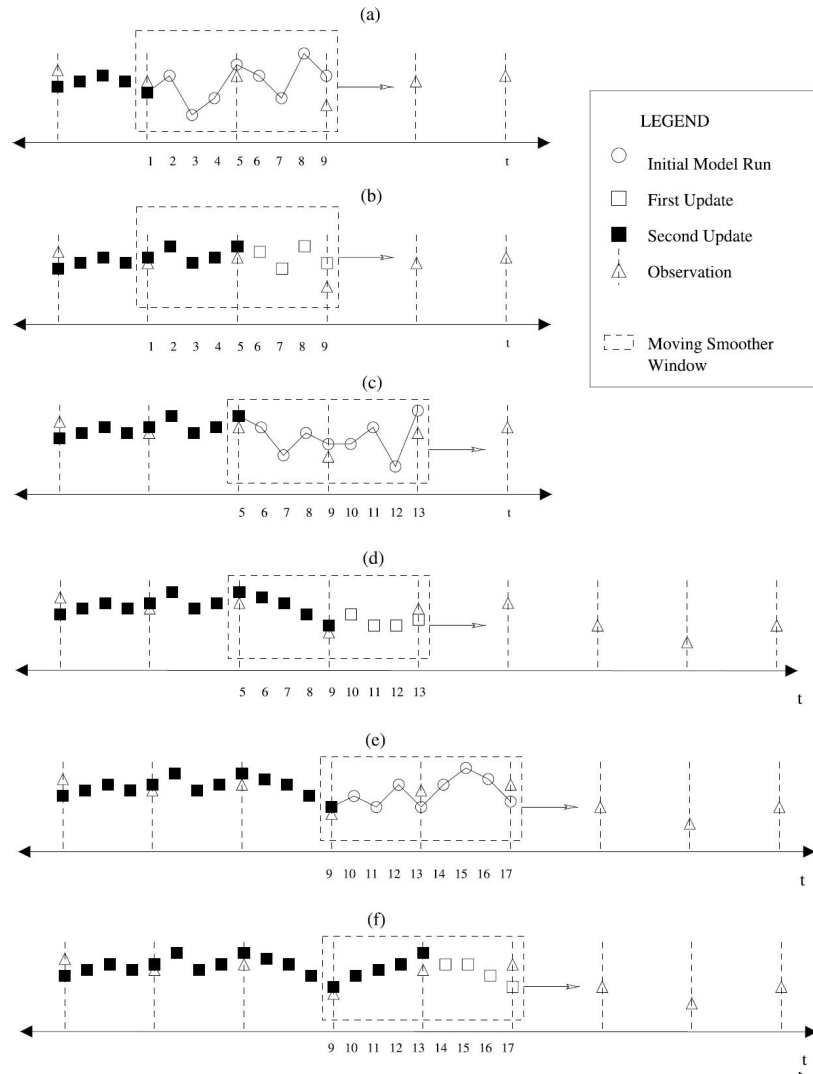


Figure 3.5: *Conceptual diagram of EnMB smoother algorithm. An estimate of the state is required at every time step, while observations are available at every fourth time step (after Dunne and Entekhabi (2005))*

The Ensemble Moving Batch Smoother is a simple extension of the EnKF in which the states are distributed in time and updated in a 'batch'. The number of observations included determines the length of the observation

vector, the state vector and consequently the covariance matrices (Dunne and Entekhabi, 2005).

In the conceptual diagram in Figure 3.5 the batch contains three observations. The smoother window refers to the interval between the first and last observation. The forward model runs through to the end of the smoother window to obtain the prior estimate of the state. An augmented state vector Y contains the states of interest (y) at all time steps of interest, which may include times at which the state is not observed.

$$Y = [y_1 \ y_2 \ \dots \ y_9]^T \quad (3.11)$$

The augmented measurement vector Z contains all the observations in the smoother window:

$$Z = [z_1 \ z_5 \ z_9]^T \quad (3.12)$$

The EnKF equations in the previous section are applied to these augmented vectors to yield an updated estimate. When the EnKF equations are implemented for a batch of observations, the covariance matrices relate the state at multiple times to all observations in the batch. The Kalman Gain matrix reflects the relevance of future observations to the current state. The smoother window is moved along the study interval one observation at a time, as including a new observation introduces new information.

In Chapter 7, where the Ensemble Moving Batch Smoother simulations are shown, there is an explanation of the EnMB used in this master thesis, and an analysis of the different parameters.

CHAPTER 4

MODEL UNCERTAINTY

4.1 Introduction

In this chapter the perturbation of the parameters is analyzed, both for the parameter model maps and for the forcing data maps. At the end of the chapter there is also the explanation of the 7 years simulation of the Ensemble Open Loop, as well as some comments of the EnsOL(Ensemble Open Loop) results.

4.2 Perturbing Parameters

The initial ensemble of data should ideally be chosen to properly represent the error statistics of the initial guess for the model state. But because of uncertainty of the nominal initial input parameters, we need to perturb these parameters. This should be done adding a normally distributed random fluctuation (Margulis et al., 2002). This will ensure that the system is in dynamical balance and that proper multivariate correlations have developed.

So, two types of maps were perturbed in this research: the parameter model maps and the forcing data maps. Both of them were perturbed in the most appropriate way as proved in the research of Widiastuti (2009).

4.2.1 Parameter Model Maps

The parameter model maps used in this thesis have the form of PC Raster maps. (Widiastuti, 2009), in her research recommended the following parameters based on her sensitivity study:

- beta: Exponent in soil runoff generation equation
- cflux: Maximum capillary rise from runoff response routine to soil moisture routine
- fc: Total water holding capacity of the soil
- Icfi: Maximum interception storage in non forested area
- Icfo: Maximum interception storage in forested area
- Ip: Fraction of field capacity below which actual evaporation = potential evaporation
- k4: Recession constant base flow
- khq: Recession rate at flow HQ
- maxbas: Number of days in unit hydrograph (≤ 10)
- perc: Exponent in soil runoff generation equation

The standard deviation of the perturbation was $dev=0.1$ of the parameter value, and the type of the perturbation size was:

$$dev = 0.1 * (maxvalue - minvalue) \quad (4.1)$$

so, standard deviation is equal to 0.1 times the range of the parameter.

4.2.2 Forcing Data Maps

In this thesis the meteorological forcing data used are precipitation, air temperature, and evapotranspiration of a daily timestep. The available data are from January 1st 2001 until December 31st 2005, and the grid size is 1 km (Widiastuti, 2009).

The form of the data is PC Raster maps and the used unit is millimeter for precipitation and evapotranspiration while for the temperature is Celsius

degrees. The precipitation data originates from observations at 46 stations that provide hourly values of precipitation. Interpolation from these point observations into the whole map was required. This was done by making use of mean monthly precipitation background grids. The measured precipitation is divided by these grids to derive the precipitation anomaly. The anomaly is then interpolated to a grid with the same size as the background grid, and then is multiplied with the background grid to derive the interpolated field. This approach take into account the orientation of the terrain and corrects for orography. The interpolation methodology was developed in Deltares (Weerts et al., 2008).

The temperature observations came from approximately 200 stations, providing hourly values of temperature. Missing temperature data at stations are filled using Kriging, using variogram parameters derived for Switzerland and taking into account the east-west direction of Alps (anisotropic variogram)(Widiastuti, 2009). Next, the temperature is interpolated to mean height of the sub-basin. Then the mean height can be used to calculate the temperature in different elevation zone using the parameter *tcalt* with a default value of 0.6, resulting in temperature maps for each time step (Weerts et al., 2008).

Potential evaporation data is derived from long term mean potential evaporation measurements from limited stations, and the potential evaporation is the same for every day of a month (Weerts et al., 2008).

For the perturbation of the forcing data maps, the method followed is the same as that used in Widiastuti (2009). In this case, exponential spatial correlation functions are used to model the spatial covariances of the forcing data. This is done to ensure that the perturbed maps maintain a reasonable spatial correlation. For example when there is precipitation at one pixel, it can be expected that precipitation also occurs in the neighbouring pixels.

In the perturbation, the spatial correlation is applied using an exponential function:

$$C(i, j) = \exp(-1 * (\frac{\sqrt{(X(i) - X(j))^2 + (Y(i) - Y(j))^2}}{L})) \quad (4.2)$$

where $C(i, j)$ is the spatial correlation, i and j denotes the row and column respectively, X and Y denotes the coordinates in X and Y direction, and L is the correlation length. The covariance matrix now becomes:

$$C_{dev} = dev^2 * (C + C^T - I) \quad (4.3)$$

where I is an identity matrix. The deviation sizes used in this master thesis are: 0.15 for the precipitation and evapotranspiration, and 0.1 for the air temperature.

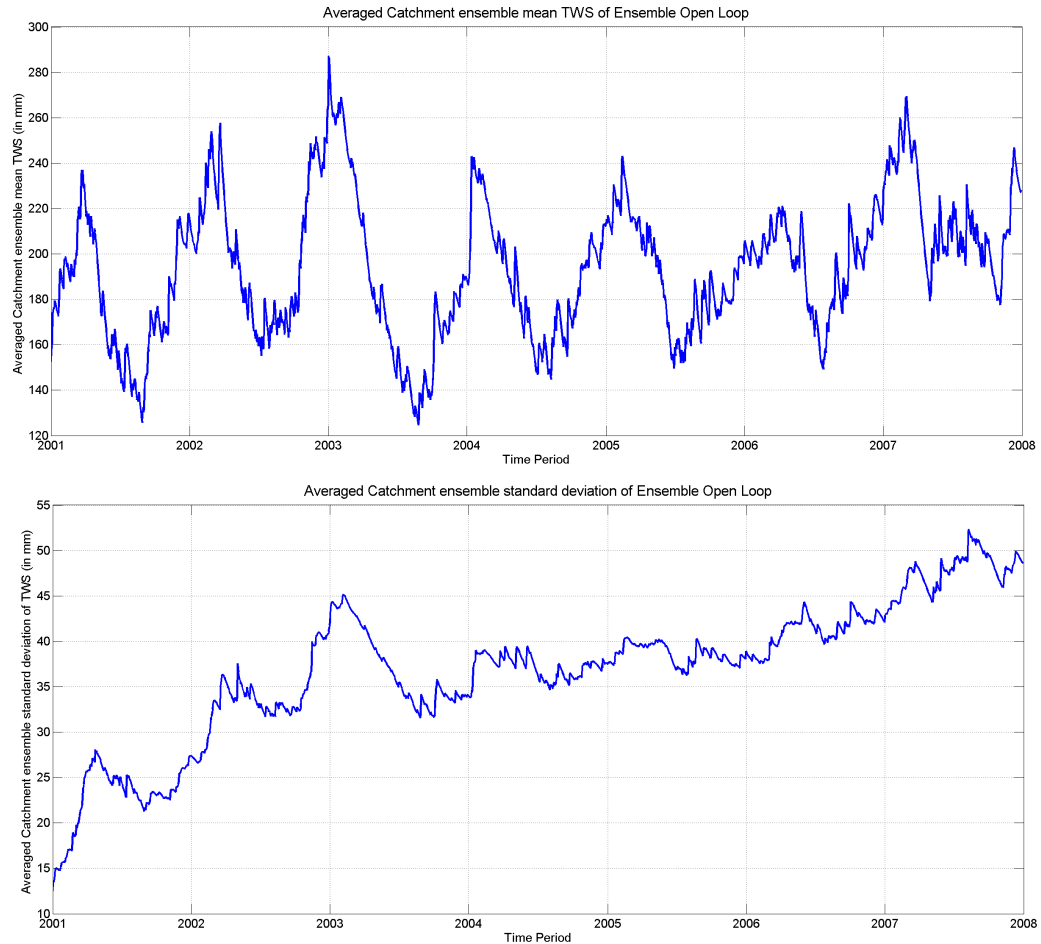


Figure 4.1: *Catchment averaged ensemble mean Terrestrial Water Storage of Ensemble Open Loop (upper plot). Catchment averaged ensemble standard deviation of TWS for Ensemble Open Loop (lower plot)*

4.3 Ensemble Open Loop

The scope of the Ensemble Open Loop(EnsOL) is to let us see how the model performs without assimilation and observations. This can be viewed as a "first" guess of the true states available without the grace GRACE observations. At the same time the first results of the EnsOL will be used

as initial conditions for the experiments. Thus the EnsOL is a way to check the effect of the uncertainty.

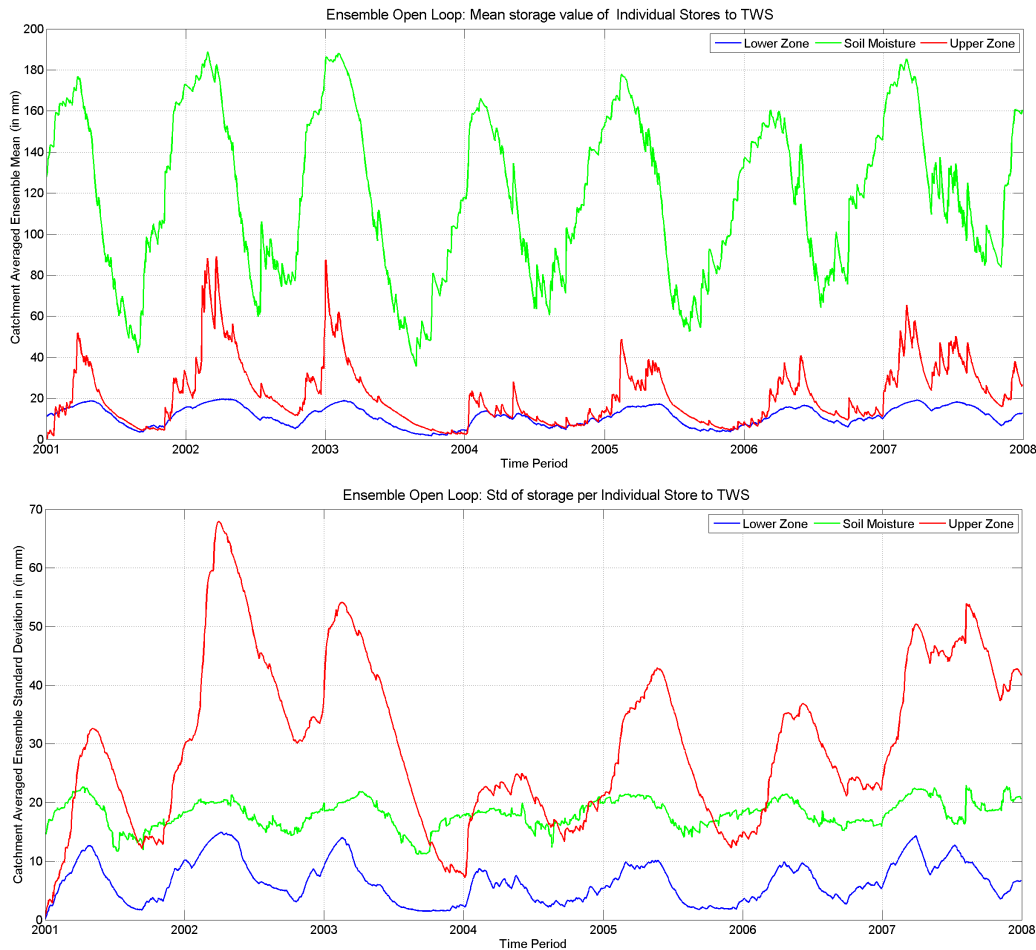


Figure 4.2: *TWS individual stores of the Ensemble Open Loop (ensemble mean and standard deviation)*

In the Ensemble Open Loop, a sample of 30 ensembles were taken. Perturbed parameters were used both for forcing data maps and forcing model maps. As mentioned earlier the data given were for a seven year period.

In Figure 4.1 we can see the catchment averaged ensemble mean TWS of the ensemble open loop and the catchment averaged standard deviation in TWS. In the upper plot we can observe that there is an annual pattern of catchment mean, which has its highest peak always somewhere between January to March, and the lowest peak in the summer season, usually at the end of it.

In the second plot, the standard deviation of the catchment for the same period, we can see that there is a continuously increasing error in the ensemble open loop, and that is because of the continuously added perturbed parameters.

The ensemble mean TWS of the Figure 4.1 is the ensemble of the model state $Y(t)$ in equation 3.8, which is the TWS (terrestrial water storage) and calculated as:

$$Y(t) = \sum (SM(t) + UZ(t) + LZ(t)) \quad (4.4)$$

where SM is the soil moisture storage, UZ is the upper zone storage and LZ is the lower zone storage.

In Figure 4.2 we see the plots of the mean and standard deviation of the individual storages of the TWS (soil moisture, upper zone and lower zone storage). It is obvious that the max values of the three stores which are determined by the HBV-96, are very important for the resulting magnitude of the individual storages of the TWS. So, as it is calibrated from the model, the soil moisture is the storage that responds faster than the other two stores. This is the reason for the high values of the soil moisture storage for the whole time span. At the same time it is characteristic of the model that the lower zone has a smooth movement for the time span. This is because the lower zone storage is the last one to be updated from the model.

In the following chapters, the Ensemble Open Loop will be analyzed furthermore compared with the Ensemble Kalman Filter, the Ensemble Kalman Smoother and the Ensemble Moving Batch Smoother results.

CHAPTER 5

INITIAL SIMULATIONS

5.1 Extending the simulation period

5.1.1 Introduction

As mentioned in the Research objectives section, the first thing to do in this master thesis is to extend the period of simulation. In the conclusions chapter of Widiastuti (2009) it was mentioned that the most important step in the data assimilation of GRACE TWS into an hydrological model using EnKF and EnKS is to perform longer simulation period. The indications of seasonality in Widiastuti's simulations, and the same indications from the Ensemble Open Loop, lead my research initially to the extension of the simulation period. This was done in order to investigate if there is a yearly repeated pattern or if the initial conditions are affecting the annual distribution of water. In this section are given the details of the implementation and afterwards there is an analysis of the results. Finally, in the last part of the section there is an analysis of a bug discovered in the simulation script and a general discussion of the extended simulation period results.

5.1.2 Implementation

In the previous chapter, when the Ensemble Open Loop simulation was done, the resulted Figure 4.1 indicated the annual pattern of catchment mean as

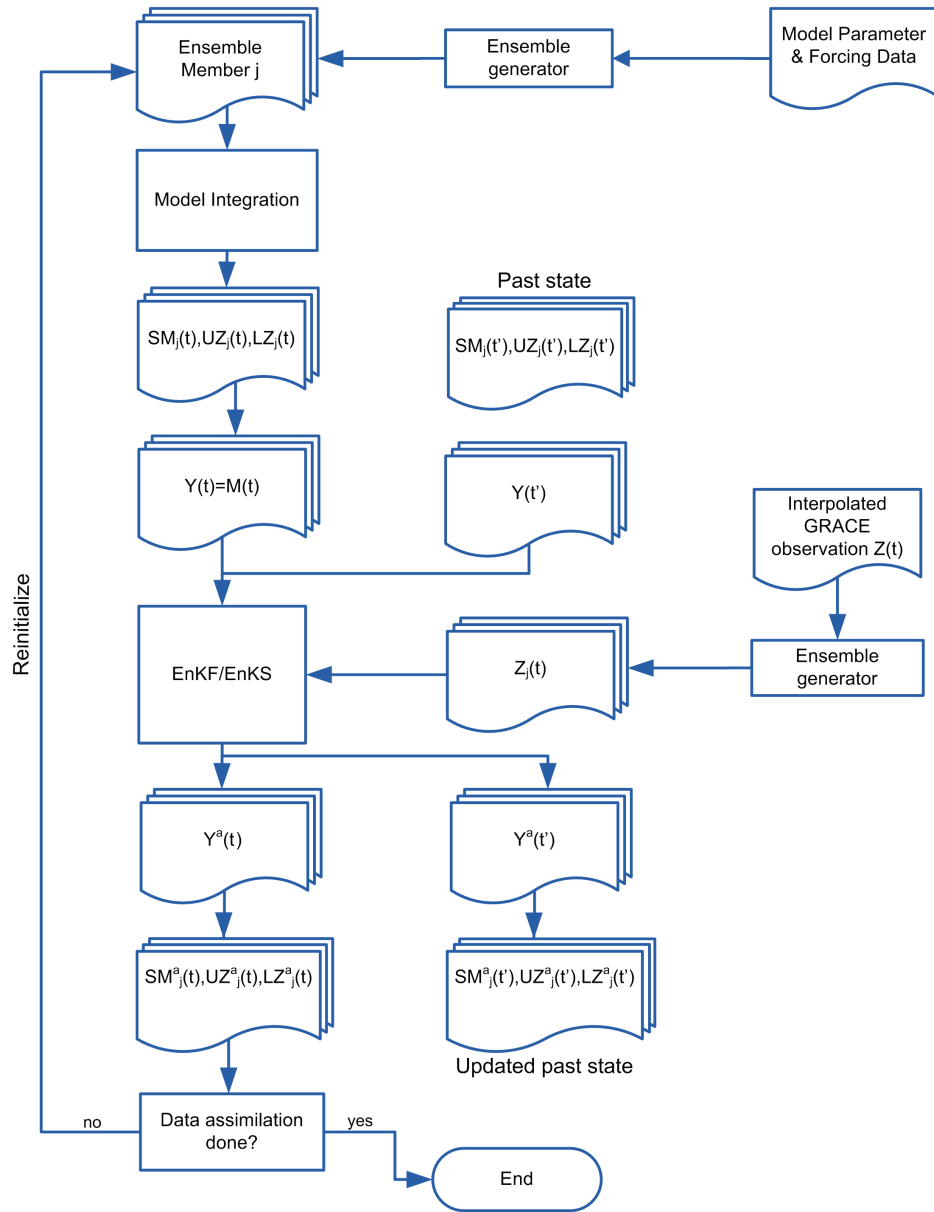


Figure 5.1: Flow diagram of the GRACE Ensemble Kalman Filter and Ensemble Kalman Smoother. SM is for soil moisture, UZ is for upper zone and LZ is for lower zone (after Widiastuti (2009)).

expected. Although simulating the EnKF/EnKS in the model could produce a different result.

In this section assimilation of the GRACE data DMT1 into the HBV-96 model for the region of Rhine river basin was done, using the EnKF

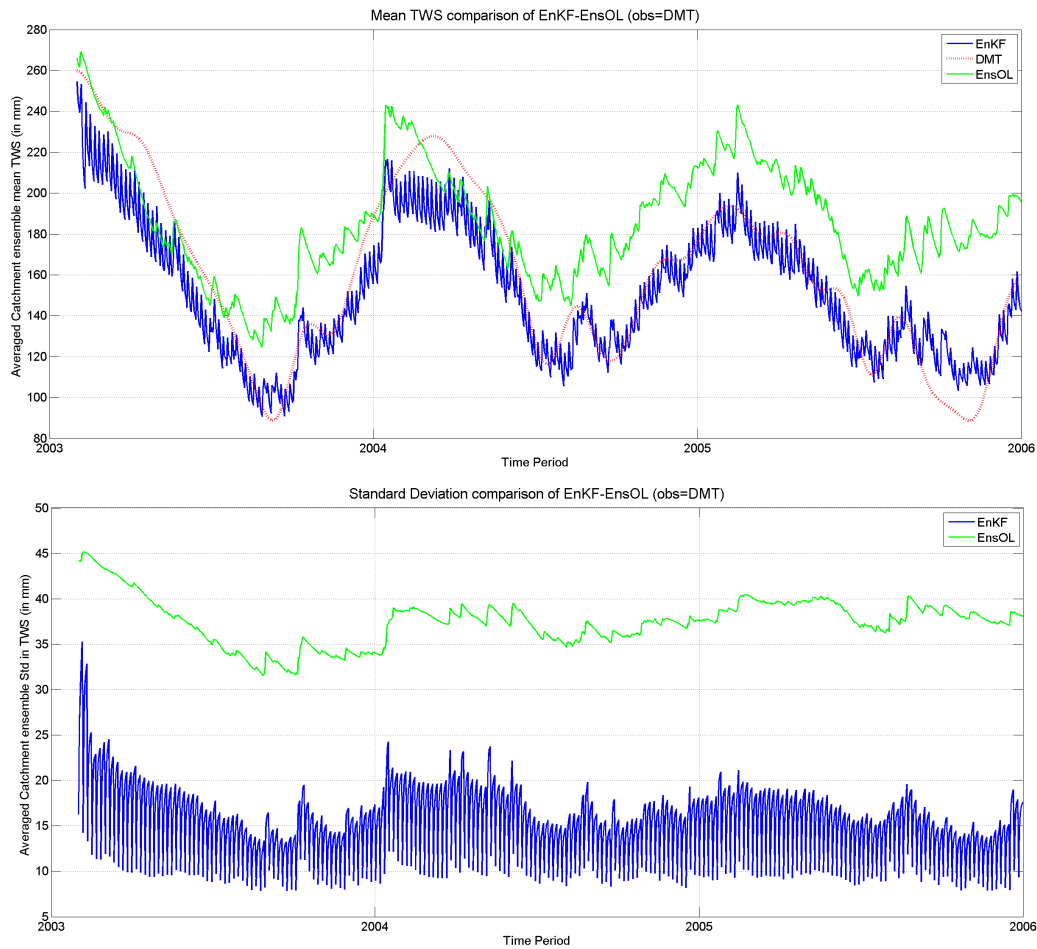


Figure 5.2: *Averaged catchment ensemble mean TWS of Ensemble Kalman Filter compared with the GRACE DMT observation dataset and ensemble mean TWS of Ensemble Open Loop (upper plot). Averaged catchment ensemble standard deviation of TWS for Ensemble Kalman Filter compared with EnsOL (lower plot).*

and EnKS filters. For the implementation of the EnKF and EnKS for the period between February of 2003 and December of 2006, the DMT1 GRACE dataset was used. As initial condition for the simulation, the first 20 days of the Ensemble Open Loop were used.

As mentioned in a previous chapter the EnKS is a straight forward extension of the EnKF because the EnKS uses the ensemble covariances timely to spread the information also backward in time Evensen (2007). In this case there are defined three different updates: *i*) lag1 is when the observation k is used to update state vector back as far as observation $(k-5)$, *ii*) lag2 is when the observation k is used to update state vector back as far as observation

(k-10) and *iii*) lag3 is when the observation k is used to update state vector back as far as observation (k-15). Those are denoted from now on simply as lag1, lag2 and lag3.

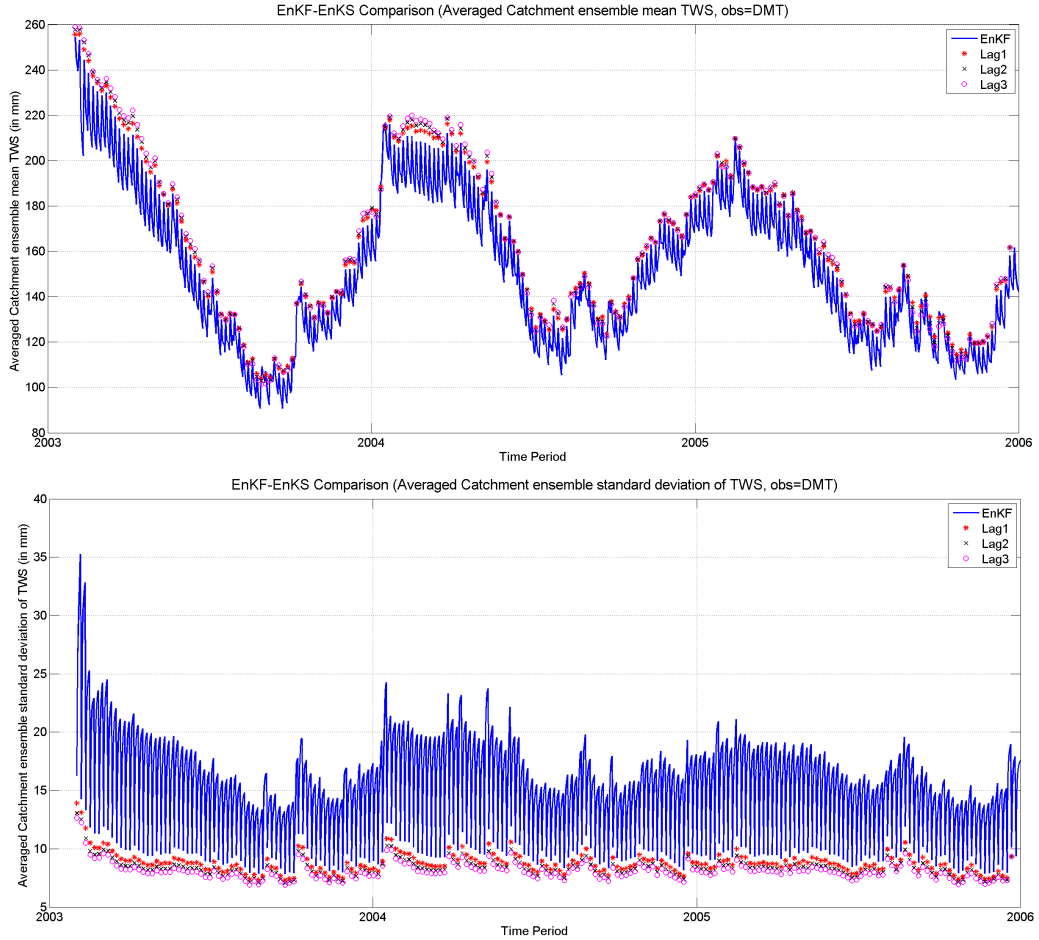


Figure 5.3: *EnKF* and *EnKS* ensemble mean *TWS* of the averaged catchment and ensemble standard deviation of *TWS*. The observation dataset used is *GRACE DMT*. The three different *EnKS* updates (5, 10, and 15 days before the update day) denoted as *lag1,2,3*

The parameters used are the same as the previous simulation of the Ensemble Open Loop. The algorithm used in the simulation is best described in the Figure 5.1 featuring the flow diagram of the algorithm.

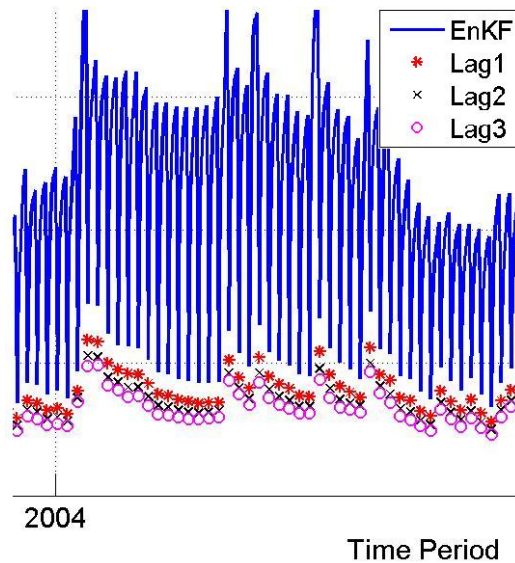


Figure 5.4: *Zoom in at the first eight months of the EnKF and EnKS simulation of the previous plot (Standard Deviation of the averaged catchment)*

5.1.3 Results

From the EnsOL already, it is understood that there is a yearly repeated pattern. In the upper part of Figure 5.2 we can see the resulting TWS estimates from the EnKF/EnKS DMT1. The yearly pattern is also occurred in the result of this simulation. Highest values in the winter time for all three years and lowest values during the dry summer period.

The effect of the initial conditions is also visible, because of the highest and lowest values through the first year. Those are because of the initial perturbation. At the highest and lowest values, the EnKF and EnKS are trying to correct the initial conditions, but through the next years the pattern is normalized, and the variation of the TWS is almost the same.

As it was expected before the simulation the Ensemble Kalman Filter is updating towards the observation through the whole time span. But also, this is the reason of the low curve in the last part of the simulation, when the observation is quite low (as shown in Figure 5.9). At this stage the variation of the mean TWS value is not so big whenever an observation is introduced. This is also visible at the standard deviation plot (lower part of Figure 5.2) when the lowest values are meet.

Also, in the lower part of Figure 5.2 the standard deviation values of the first year are higher compared with the sequential years. That is once again

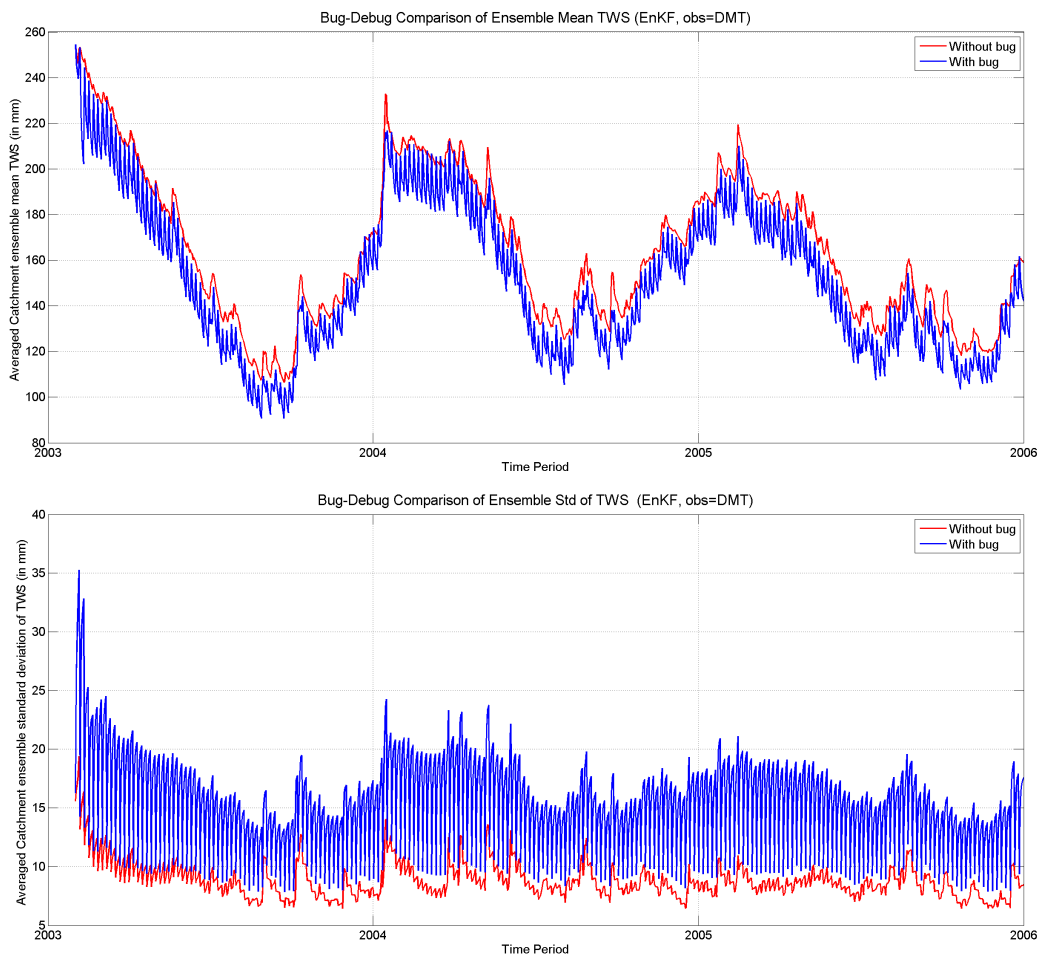


Figure 5.5: *Bug-Debug comparison of Ensemble Kalman Filter (in mm)*

because of the initial conditions. Also every winter time there is a bit of a rise in the standard deviation, and that is because of the season's rainfall when the individual stores are full of water. It is also worth mentioning that the standard deviation values are almost for the whole simulation period, except from the initialization period, under the critical 20mm GRACE accuracy.

The standard deviation in the lower part of Figure 5.2, every time that there is an update it grows rapidly. This "sawtooth" pattern is probably because of a bug in the code which leads to a mistake in the update of the state vector.

In the Figure 5.3 we can see the results of the EnKS. The lag1, lag2 and lag3, are mostly following the GRACE observations as it is visible in catchment mean plot. At the same time they have lowest standard deviation

than the EnKF solution, and as the smoother works backwards in days, the lowest standard deviation we get, and so as a result the lag3 is the lowest.

Finally in Figure 5.4 a detail of the Figure 5.3 is shown. It is a zoom in at the first eight months of the EnKF and EnKS simulation. In this figure is clear how the Ensemble Kalman Smoother improves the result as the observation k is used to update state vector as back as possible. As far as the $k-15$ is working perfectly, smoothing the simulation result and at the same time obtaining lower standard deviation.

5.2 Debugging

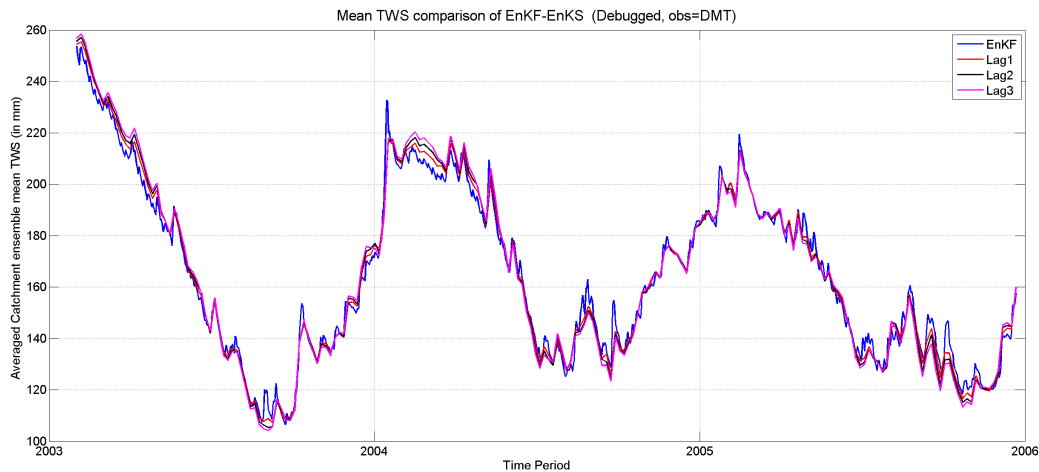


Figure 5.6: Debugged EnKF and EnKS ensemble mean TWS of the averaged catchment. The observation dataset used is GRACE DMT. The three different EnKS updates (5 days step) denoted as lag1,2,3

In the initial implementation of the algorithm, the produced results had a minor anomaly. In every step, where an observation from the GRACE dataset was involving in the simulation the catchment-averaged mean TWS was increasing by 10 – 20mm approximately, as it is obvious in the upper part of Figure 5.2; and also the standard deviation has the same "sawtooth" reaction to it as we see in the lower part of Figure 5.2.

After several tests and tries, a bug was found in the script, through the update process. Debugging the code, the results are really promising, as it is shown in Figure 5.5. In those two figures there is comparison of the catchment mean and standard deviation of those two simulation. The behavior of

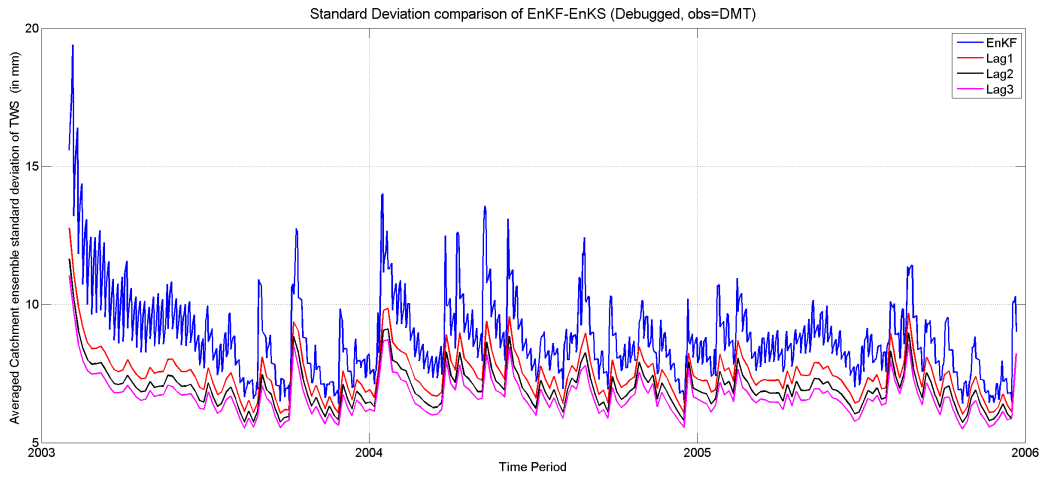


Figure 5.7: Debugged *EnKF* and *EnKS* ensemble standard deviation of the TWS for the averaged catchment. The observation dataset used is GRACE DMT. The three different *EnKS* updates (5 days step) denoted as lag1,2,3

the debugged version seems more normal and more close to what was expected. The standard deviation of catchment is almost the half of the bugged standard deviation. It is always close to 10mm.

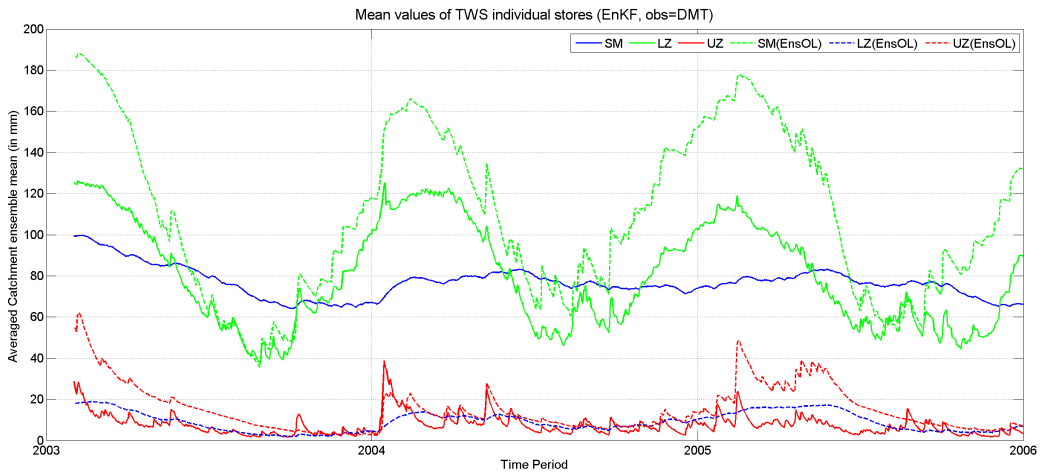


Figure 5.8: Individual stores (*Upper zone, Lower zone and Soil moisture*) of the averaged catchment after de-bugging compared with *Ensemble Open Loop* individual stores (in mm)

In Figure 5.6 we can see that the *EnKS* has the same effect in the debugged version as it has in the bugged version. The lag1, lag2 and lag3, are mostly following the GRACE observations and the standard deviation of

debugged simulation is even lower in this case, where lag3 has always close $6 - 8 \text{ mm}$ of standard deviation.

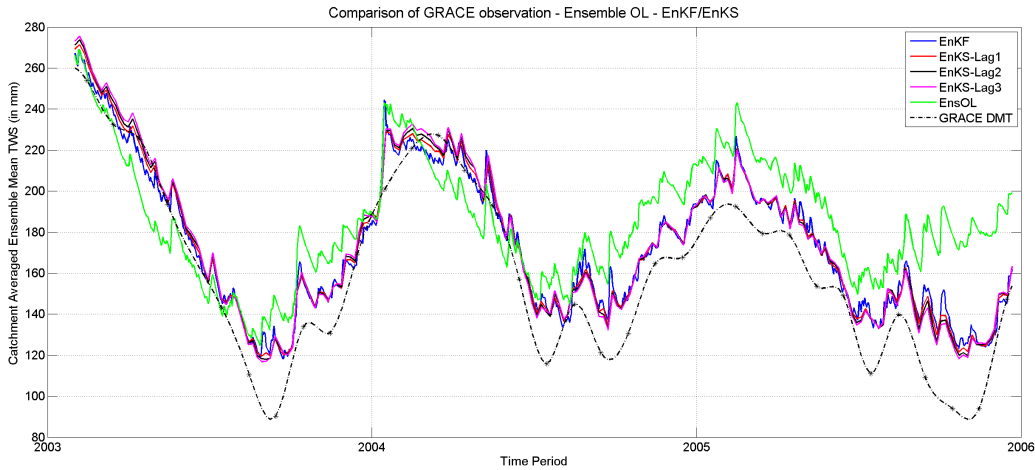


Figure 5.9: Averaged catchment mean TWS (in mm) for: Ensemble Open Loop, Ensemble Kalman Filter, Ensemble Kalman Smoother with three different steps denoted as lag1,2,3. All compared to GRACE observation (DMT algorithm).

In Figure 5.8 the individual contributors of the TWS are shown. In this figure we can see that the soil moisture is following mostly the pattern of the ensemble mean TWS and also has the highest peaks. The lower zone has also high magnitude compared to the upper zone which has lower values and also is not following the TWS pattern. But we can see that in the winter season where the catchment mean is increasing, also the upper zone has its highest peaks.

In the same Figure 5.8, the contributors of the Ensemble Open Loop results are also plotted. It is the first comparison of the different layers between the model and the simulation. The EnKF results seem to react as expected in the simulation. Except from lower zone which is significantly higher than the Ensemble Open Loop results. This might be an indication of mistreat on the limitations of the lower zone value. Also the EnKF soil moisture layer is not reaching the high values of the EnsOL.

In Figure 5.9 the comparison between GRACE observation, Ensemble Open Loop, Ensemble Kalman Filter and Ensemble Kalman Smoother is shown. The GRACE observation is the DMT algorithm dataset. For the EnKS three different updates are used denoted as lag1, lag2 and lag3.

5.3 GRACE Algorithms Comparison

5.3.1 Introduction

To understand the effect of different algorithms applied in the GRACE data, there were used three different datasets in this master thesis. Firstly the already used DMT but this time extended from February of 2003 until February of 2009, the second one is the CSR covering a period between February of 2003 until December of 2009, and finally the RBF dataset, which covers a period between February of 2003 and December of 2006.

The same method used for all three datasets in the implementation which lead to the result given latter on. Finally in the next section of the chapter there is a discussion about the commonalities, differences of those three datasets and the effectiveness of them when used with the Ensemble Kalman Filter and the Ensemble Kalman Smoother.

5.3.2 Implementation

In section 2.4, the different algorithms of the GRACE observations were analyzed. In this part of my master thesis, those three different GRACE datasets (DMT, CSR, RBF) are assimilated into the HBV-96 model for the region of Rhine river basin, using the EnKF and EnKS filters. This was done for the period between February of 2003 and December of 2006. As initial condition for the simulation, the first 20 days of the Ensemble Open Loop where used for all three cases.

Before implementing those three different GRACE datasets a change was done in the disaggregation of the TWS, because the prior disaggregation of the TWS didn't have logical sequence. Due to the minor effect on the result and because of the importance of this change on the state vector research, it is analyzed in chapter 6, and section 6.1

5.3.3 Results - Discussion

After simulating the DMT dataset the other two data sets where used for the simulations. All the three simulations were done following the same flow diagram (presented in Figure 5.1).

The results of those simulations are shown in Figures 5.11 and 5.12. Figure 5.11 is the averaged catchment ensemble mean TWS and Figure 5.12

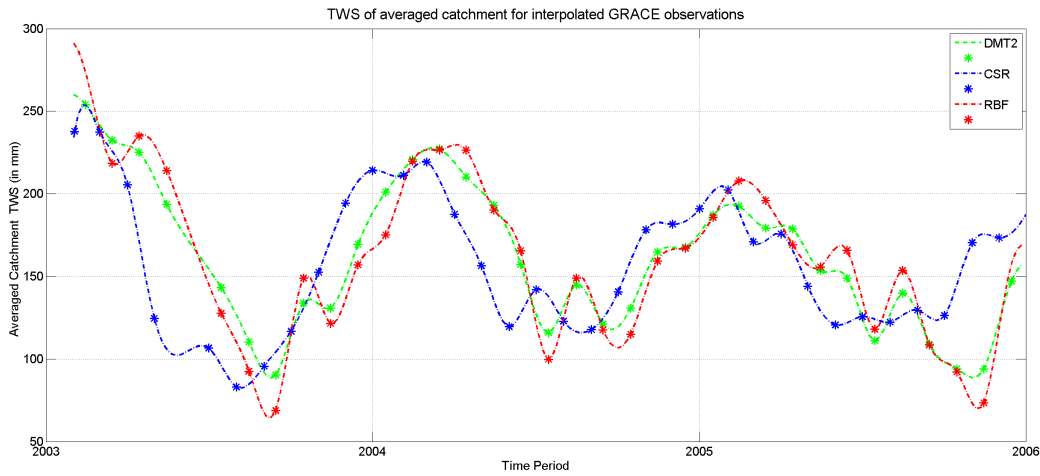


Figure 5.10: Comparison of the three datasets of GRACE Observations, DTM, RBF and CSR (TWS averaged catchment in mm)

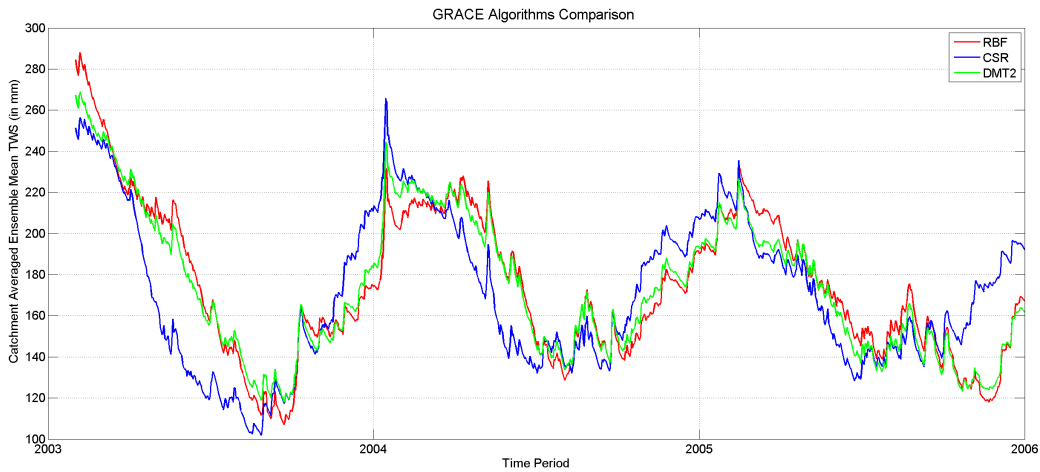


Figure 5.11: Comparison of the different GRACE algorithms. Ensemble Kalman Filter was used for the mean of the TWS averaged catchment in mm

is the averaged catchment ensemble standard deviation of TWS, after the assimilation of GRACE data into the HBV model using EnKF.

To be able to compare those results with the GRACE observations, in Figure 5.10 the differences in time of the three datasets before the simulations are plotted.

Clearly there is a distinction between CSR and the other two algorithms. At the mid-season of each year the simulation with the CSR algorithm is producing less water than the other two in the averaged catchment. This

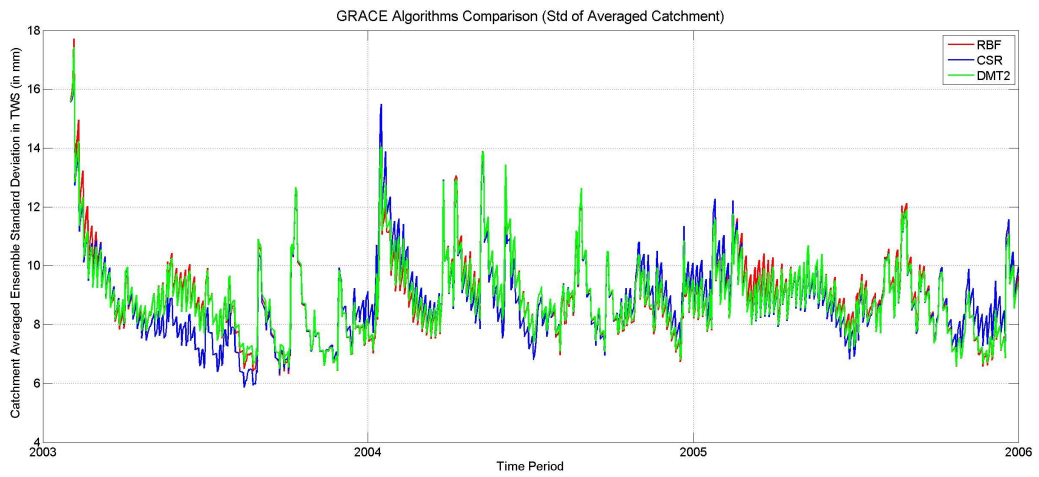


Figure 5.12: Comparison of the different GRACE algorithms. The standard deviation of the of the TWS averaged catchment in mm (Ensemble Kalman Filter)

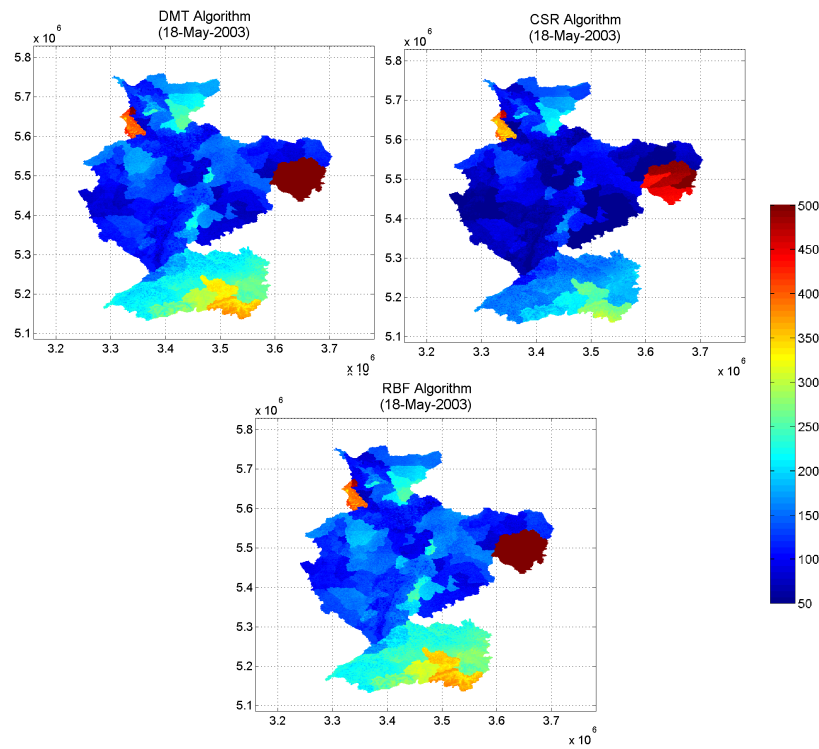


Figure 5.13: The three different algorithms compared for the 18-May-2003, simulated using the Ensemble Kalman Filter (Catchment in mm)

difference is more clear in the first year of the simulation while in the following years is not so tense. This is probably because of the initial conditions. Also

at the end of each season, the CSR not only covers the water balance between all the three algorithms, but it also overcomes the other two and produces more water in the averaged mean. This phenomena it seems to get more intense through the years. Once again this is also probably because of the initial perturbed conditions.

In Figure 5.13 the resulted TWS is plot for all three datasets for May 18th of 2003. This day was selected in purpose, as it is one of the days that the difference between CSR and the other two algorithms is quite significant. Those lower values of the whole catchment for the CSR dataset lead the mean catchment value to be lower.

The RBF and DMT dataset as shown in Figure 5.11 and 5.13, seem to have similar attitude and they seem to react with the same way in the season changes. Also, annually, those two datasets seem to have very similar pattern of the mean TWS value of the averaged catchment.

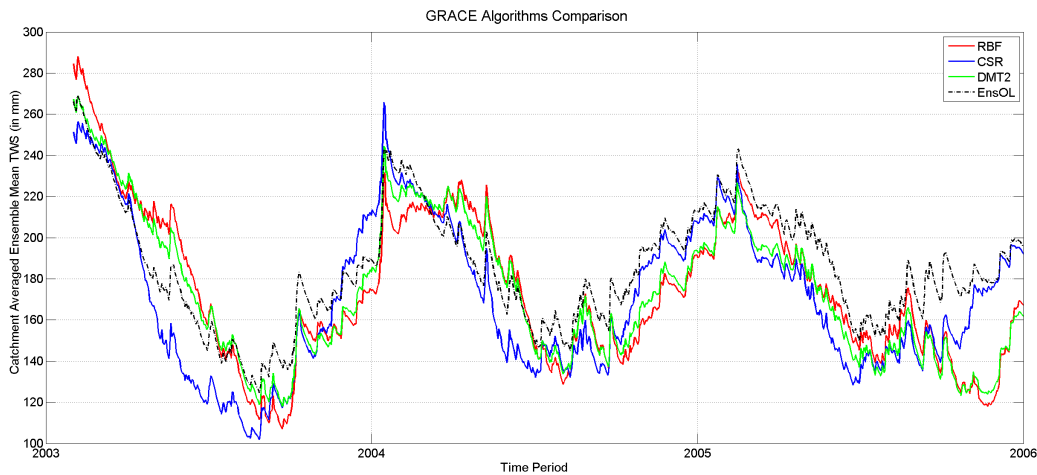


Figure 5.14: *The three different algorithms (simulated using the Ensemble Kalman Filter) compared with the Ensemble Open Loop (TWS averaged catchment in mm)*

The standard deviation values (as presented in Figure 5.12) of the three datasets are similar, and they follow the same pattern for the whole period of the simulation. The highest peaks of the simulation for the standard deviation is in the rain season of each year when the EnKF is dealing with the high rainfall. In the early steps of the first year the standard deviation is more than twice bigger than the standard deviation in the dry season. That is because of the perturbed parameters of the initial conditions which are introduced in the first steps. Generally the values are between six and thirteen.

In Figure 5.14, the resulted values of the three datasets are compared with the Ensemble Open Loop mean value of the averaged catchment. This figure could be compared with Figure 5.10, to understand why the different GRACE observation algorithm are reacting in this way when they are assimilated into the HBV model. In Figure 5.10 the interpolated values of the three GRACE observation datasets are presented. It is clear how the resulted values are affected from the observation datasets to produce the result after the simulations.

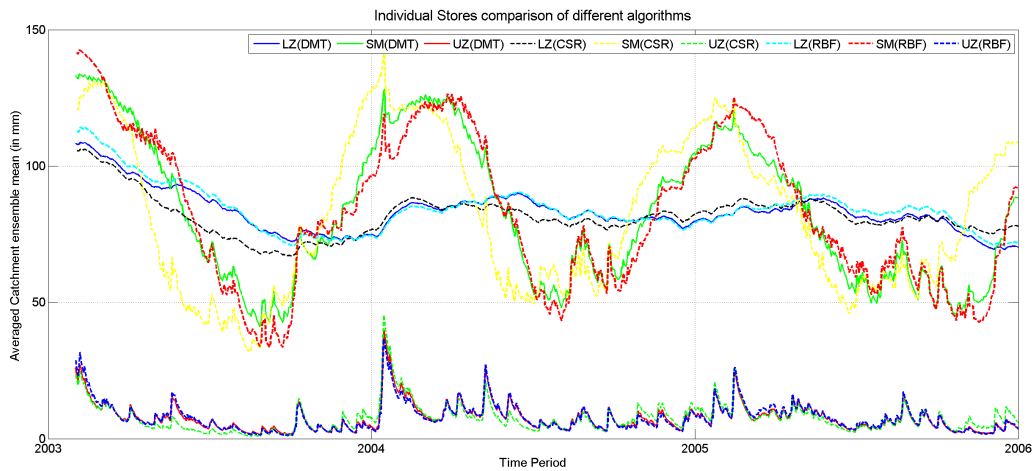


Figure 5.15: Comparison of the individual stores for the three different algorithms (simulated using the Ensemble Kalman Filter)(ensemble mean for averaged catchment per store in mm)

In Figure 5.15 a comparison of the individual stores for the three different algorithms is shown. In this plot the difference between CSR and the other two algorithms (DMT and RBF) could be explained. The difference is mostly because of the difference in the soil moisture, but also minor changes are shown in the lower zone.

CHAPTER 6

DEFINITION OF STATE VECTOR

In this chapter there is an analysis of the state vector and how it is updated. Different approaches are explained and implemented. In the first section the same method as Widiastuti (2009) was used, but there was a change in the Terrestrial Water Storage disaggregation, while in the second section the state vector change, and the three individual layers are updated individually.

6.1 State Vector Disaggregation Change

6.1.1 Introduction

When the first simulation of this master thesis was done, it was realized that the disaggregation sequence of the updated state vector was hydrologically incorrect. So, after de-bugging the code (as presented in section 5.2) and before the different GRACE algorithms comparison (as presented in section 5.3) a change to this sequence was made. Through this section this change is analyzed in depth and the the results are compared.

6.1.2 Implementation

In the previous chapter three stages of different simulations were explained and analyzed; the extension of the simulation period of the experiment, the debugging of the code which resulted in a more reasonable result and the different GRACE algorithm comparison. In between the debugging stage

and the GRACE algorithm comparison, an experiment for the state vector was done.

In Figure 5.1 where the flow diagram for the Ensemble Kalman Filter is shown, the input of the state vector of EnKF is the $M(t)$. So, the state vector $Y(t)$ consists of the TWS of the catchment. After the update of the state vector, the resultant $Y^a(t)$ is disaggregated between the different layers. This sequence until now was $SM \rightarrow LZ \rightarrow UZ$ (Widiastuti, 2009). Firstly the soil moisture layer was filled, then the lower zone and finally the upper zone. The strange sequence, that it was first the lower zone and then the upper zone, was probably because of the inability to set a maximum limitation for the upper zone layer. In this section, the sequence was changed into $SM \rightarrow UZ \rightarrow LZ$, and a maximum limitation for the upper zone change was set, as explained below. The change is presented schematically in Figure 6.1.

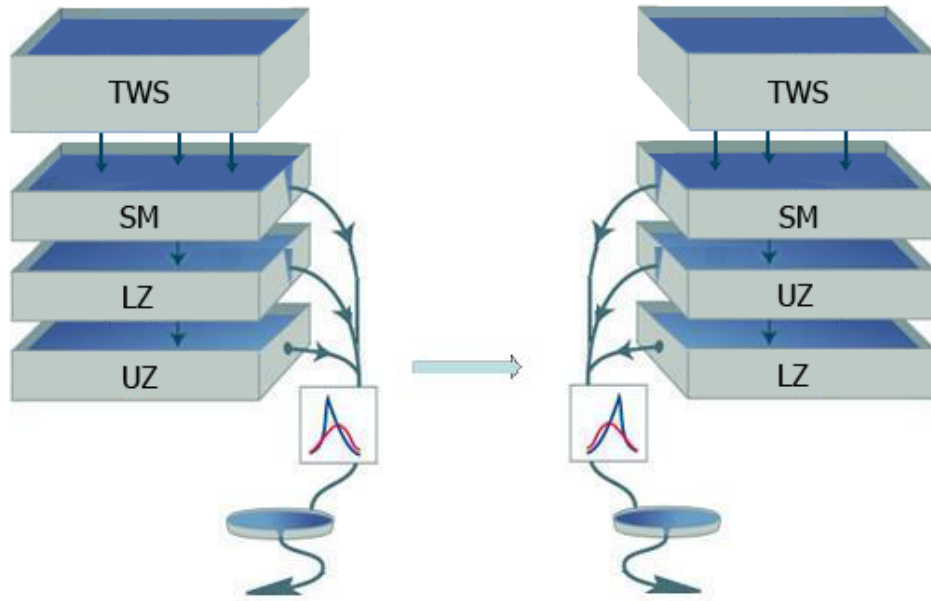


Figure 6.1: Schematic view of the state vector change. In prior simulations the updated TWS was disaggregated into SM-LZ-UZ, while afterwards the sequence was changed into SM-UZ-LZ.

In previous simulation the maximum limitations used for each layer were:

- for the soil moisture the field capacity is used as maximum limitation
- for the lower zone layer, the equation of the limitation is: $LZ_{max} = (k4/perc) * LZ_{old}$, where LZmax is the lower zone maximum limitation,

$k4$ is the recession constant (as defined by the HBV model), $perc$ is the percolation from upper to lower zone (mm/day) (Weerts, 2010)

- for the last layer in the sequence the upper zone there is no maximum value

For the new simulation the maximum limitations used for each layer were:

- for the soil moisture the already used field capacity is also used
- for the upper zone layer, the maximum value which is the 110% of the previous upper zone value. So, it is the change of the upper zone that is limited
- for the last layer in the sequence the lower zone there is no maximum value

From the state vector disaggregation change it is expected to see differences on the magnitude of both upper and lower zone. There is also the possibility to see differences in the resulted terrestrial water storage of the averaged catchment. To assimilate the data, Ensemble Kalman Filter is used for both of the simulations. The observation data are created using the DMT algorithm.

6.1.3 Results - Discussion

In Figure 6.2 the different results of the simulations for the different disaggregation of the updated state vector is shown. The lines are almost identical with minor changes in the initial part.

This denotes that the result is not affected by the sequence of lower and upper zone. The maximum limits of the layers are reached and the layers are filled in the updates. So either if the lower zone is first or the upper zone it doesn't make any difference to the TWS.

In Figure 6.3 the standard deviation for the same two simulations is shown. The result is almost identical, as expected after Figure 6.2. Minor differences are apparent in the initial part of the simulations and also during the rain season of 2005.

In Figure 6.4 the individual stores are compared. While the TWS may not change, we need to see if the individual stores are different. Also from

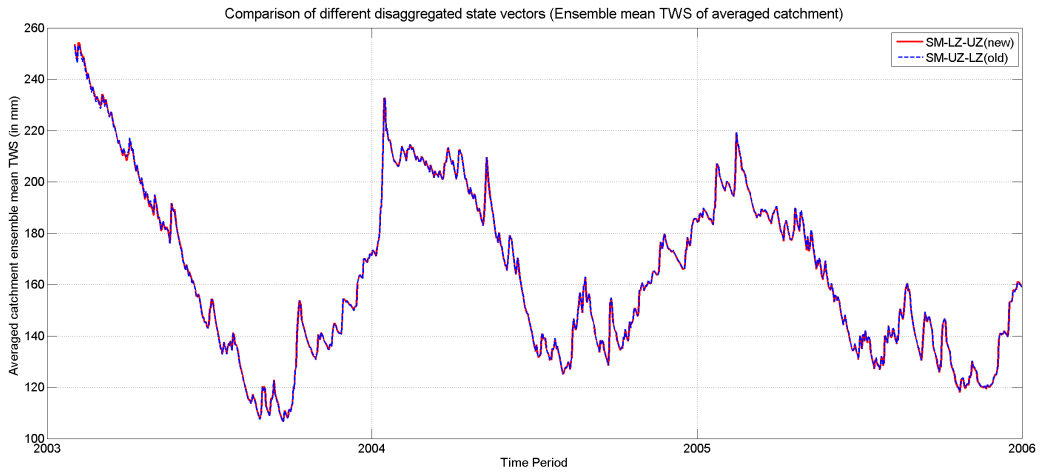


Figure 6.2: Ensemble mean TWS value of the averaged catchment for both of the simulations. In prior simulations the updated TWS was disaggregated into SM-LZ-UZ, while afterwards the sequence was changed into SM-UZ-LZ

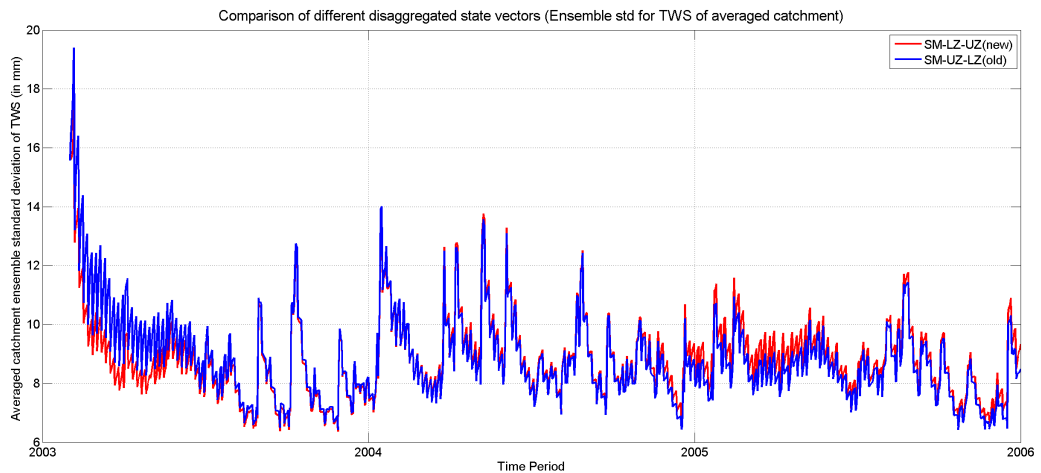


Figure 6.3: Averaged Catchment ensemble standard deviation of TWS for the simulations. In prior simulations the updated TWS was disaggregated into SM-LZ-UZ, while afterwards the sequence was changed into SM-UZ-LZ

this figure is understandable that the change between the simulations is not significant and only in some parts, differences are shown. Like in previous plots, also here in the initial part there is a minor change of lower and upper zone between the simulations.

In section 5.2, it was discussed that the lower zone has a suspiciously high value. In Figure 5.8, it was compared with the Ensemble Open Loop and it

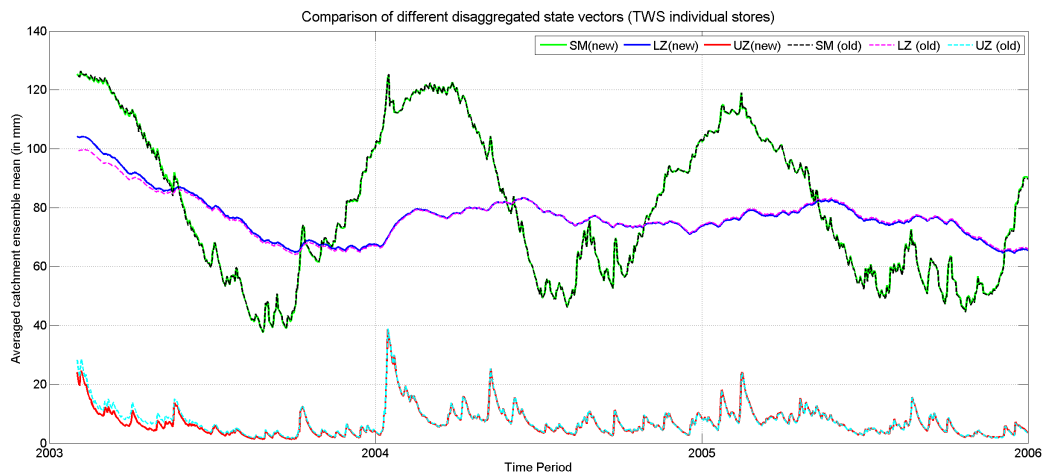


Figure 6.4: Comparison of the individual stores for both of the simulations. In prior simulations the updated TWS was disaggregated into SM-LZ-UZ (old), while afterwards the sequence was changed into SM-UZ-LZ (new)

was concluded that there is something wrong with the lower zone maximum limitation treatment in the code of the simulation. Also here in Figure 6.4, it seems that regardless of which store is limited, the lower zone still has high value. This means that there is a possibility that the maximum limits are not implemented as they should be. In the following section this bug is identified and corrected.

6.2 State Vector Change

6.2.1 Introduction

The need for a more hydrologically correct update of the state vector lead to this section of the chapter. In this section of the master thesis the change of the state vector is analyzed. The different layers are now in the state vector and they update individually. At the same time the maximum limitation check of the layers is corrected and explained.

6.2.2 Implementation

Until now the terrestrial water storage was updated in the state vector and it was using the methods explained. Afterwards it was disaggregated between

the individual TWS stores as shown in previous section. The next experiment which was done, was to update the layers individually. So, the different layers (soil moisture, upper zone and lower zone) were added in the state vector.

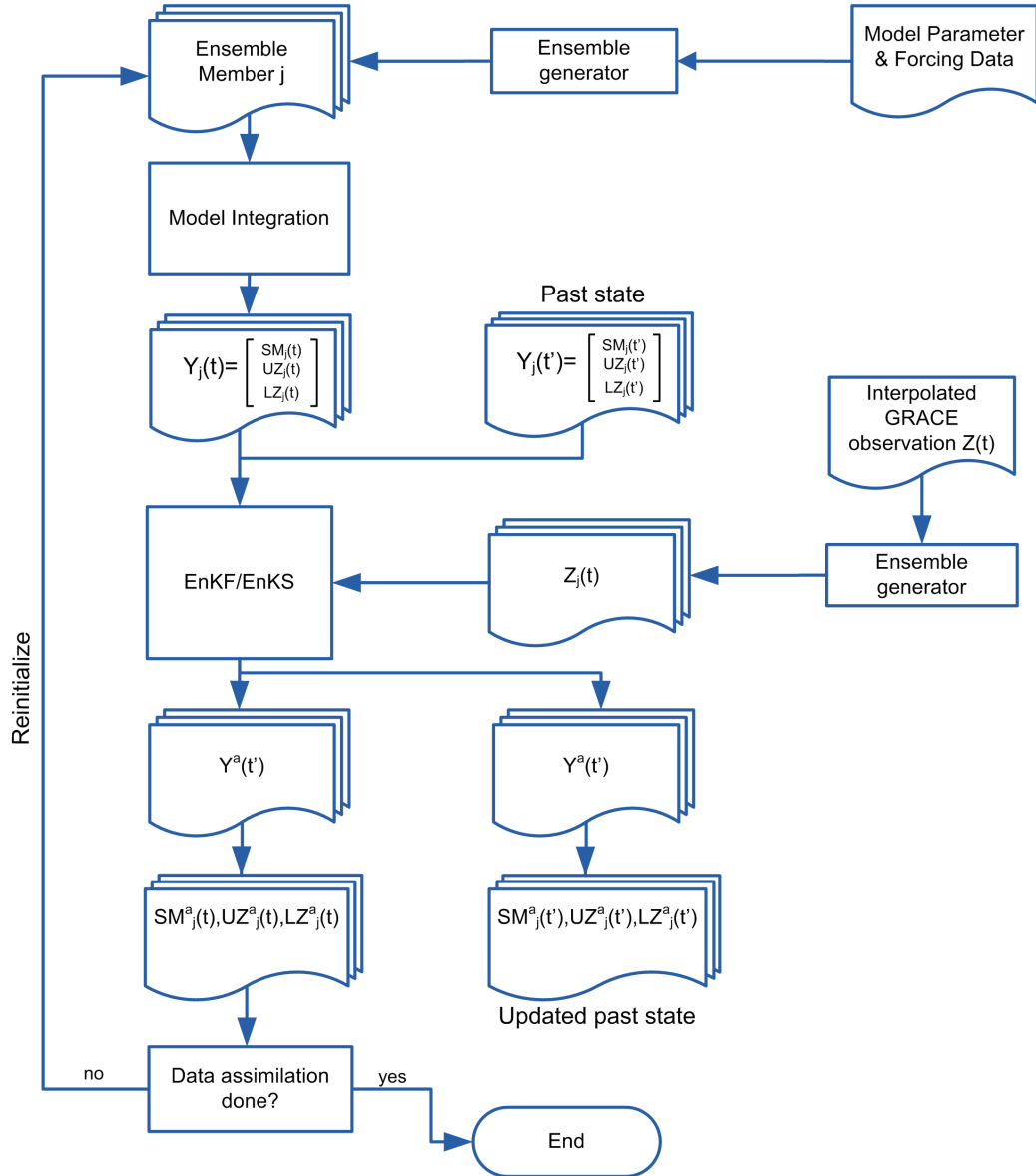


Figure 6.5: Flow diagram of the Ensemble Kalman Filter and Ensemble Kalman Smoother simulation with the new state update vector. SM is for soil moisture, UZ is for upper zone and LZ is for lower zone.

As shown in the flow diagram in Figure 6.5 the state vector in this simulation consists of the three layers and so the update is done individually for

the three different layers (Soil Moisture, Upper Zone and Lower Zone).

After the update the maximum limitations are checked. The maximum limitations are almost the same as in previous section and they are explained below:

- For the soil moisture the maximum value is the field capacity
- for the upper zone layer, the maximum value which is used is the 110% of the previous upper zone value. So, in essence it is the change of the upper zone that is limited
- the maximum limit for the lower zone layer is also based in the change. The equation of the limitation is: $LZmax = (k4/perc) * LZold$, where LZmax is the lower zone maximum limitation, $k4$ is the recession constant base flow (as defined by the HBV model), $perc$ is the percolation from upper to lower zone (mm/day) (Weerts, 2010)

As already commented in section 5.2, there was an indication of mistreat on the maximum limitations of the lower zone value. This was commented because, as shown in Figure 5.8 the lower zone was significantly higher compared with the Ensemble Open Loop results. In previous section, in Figure 6.4, it was proved that with or without the lower zone limitation the result was the same. This suggested that there may be a bug in the original Matlab code. This bug was corrected and the maximum limitations in this simulation are implemented correctly.

6.2.3 Results - Discussion

The result of the simulation is shown in Figure 6.6. Ensemble Kalman Filter and Ensemble Kalman Smoother were applied for the data assimilation, while the GRACE observation dataset was created with the DMT algorithm. In the upper part where the mean of the averaged catchment is plot, the annual pattern is followed once again but this time the spikes in the start of each season are more tense.

Also, at the end of the third year the result is not it was in previous simulations. The Ensemble Kalman Smoother works as expected with the three different updates (lag1 for k-5 days, lag2 for k-10 days and lag3 for k-15 days) to be more close between them than previous simulations.

In the lower part of Figure 6.6 the standard deviation is shown. The values are very low compared with previous plots. Actually, compared with

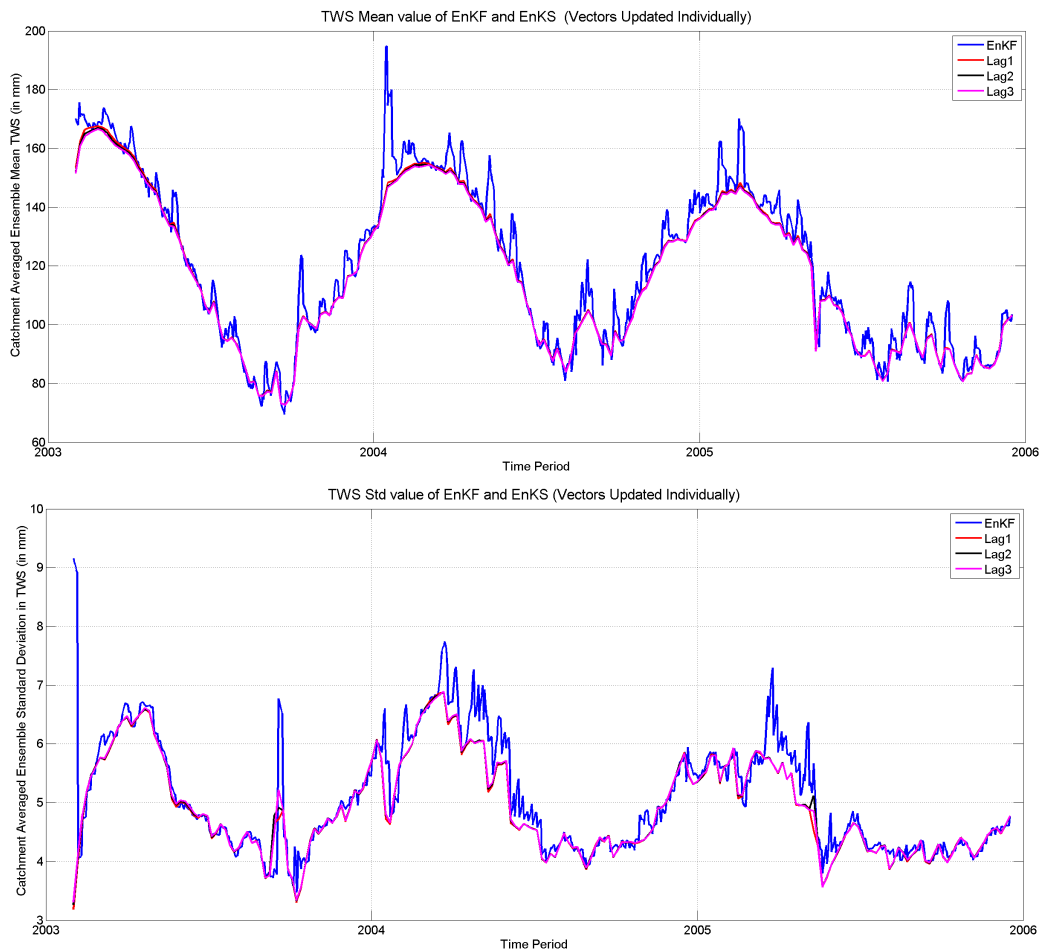


Figure 6.6: *Ensemble Kalman Filter and Ensemble Kalman Smoother assimilating the DMT observation data where the layers are updated individually. Ensemble mean TWS and ensemble Standard deviation of TWS for the averaged catchment*

Figure 6.3, it has more than half of the the magnitude and it seems to be more smooth for the whole time span.

In Figure 6.7 the contributors of the simulation are plotted and compared with the contributors of the Ensemble Open Loop. In Figure 6.8 the contributors of the simulation are plotted and compared with the contributors of the previous simulation which had the old state vector.

The soil moisture layer of the simulation with the new state vector it is more close to the values of the Ensemble Open Loop as it is shown in Figure 6.7. Although the magnitude of them is not the same; the high and low values of the Ensemble Open Loop are more extreme. Compared with

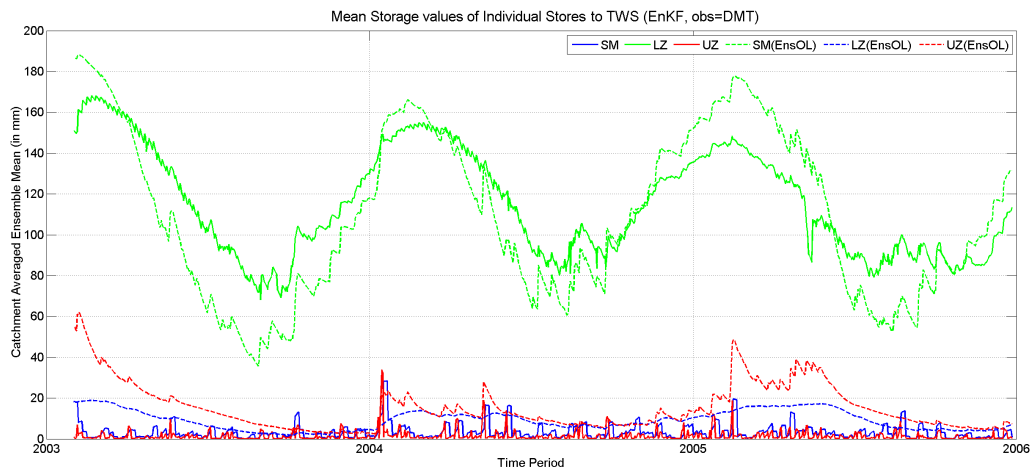


Figure 6.7: Individual stores update compared with the Ensemble open loop. SM is for soil moisture, UZ is for upper zone and LZ is for lower zone.

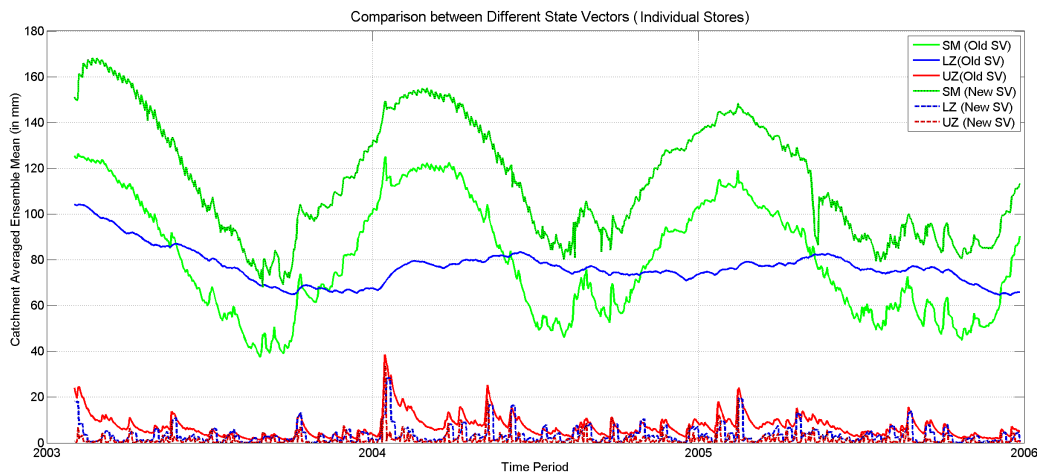


Figure 6.8: Individual stores comparison between the EnKF simulation with (New SV) and without (Old SV) individual update of the layers. SM is for soil moisture, UZ is for upper zone and LZ is for lower zone. Also, SV is for state vector.

Figure 6.8 the soil moisture is significantly raised but it follows the same annual pattern.

The upper zone of the simulation with the new state vector is lower than the previous simulation (Figure 6.8) and even lower when compared with ensemble open loop (Figure 6.7).

Finally the problem of the lower zone which was commented in section 5.2 and also in the previous one is solved. The lower zone is quite low compared

even with the Ensemble Open Loop. This indicates that previously when the vector wasn't updating individually the zones but it was updating the TWS and then disaggregated it into the layers was not correct.

But, the main problem still remains the maximum limitation of the layers. The values of the lower and upper zones seem to be quite low compared to the Ensemble Open Loop, but correct (if compared with the previous simulation). This problem will be also in concern in the next chapter, when the maximum limitations are going to be changed and tested using the Ensemble Moving Batch.

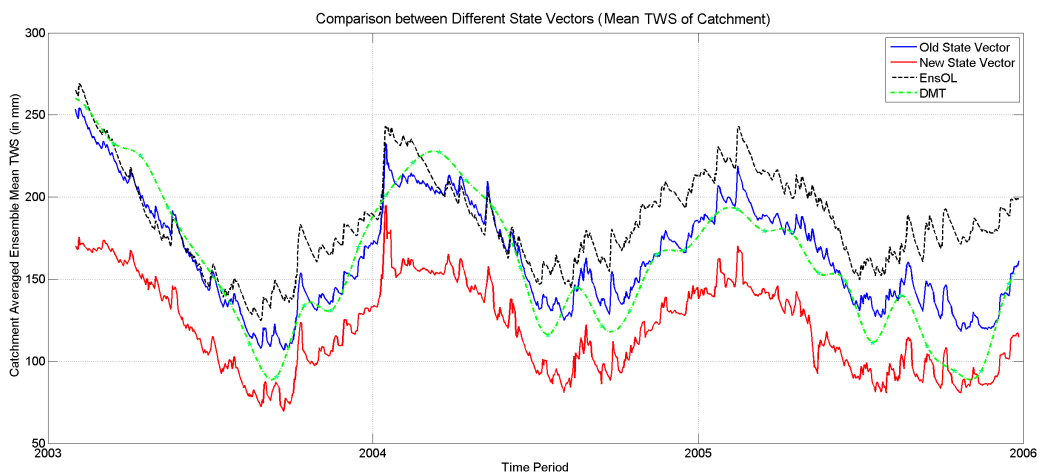


Figure 6.9: *Terrestrial Water Storage comparison between the Ensemble Kalman Filter simulation with individual update in state vector (new) and without individual update (old), with the Ensemble Open Loop and DMT observation*

In Figure 6.9 the comparison between the two different versions of the state vector with the Ensemble Open loop and the GRACE observation (DMT algorithm). When the layers are updated individually, it seems that the total amount of water which is stored in the system is lower. The previous simulation seem to be more reasonable, but the pattern which is followed seems to be the same between the two simulations.

So, the problem of the limitations for the lower and upper zone seems to affect the total amount of stored water. As mentioned earlier, in the next chapter there will be an experiment concerning the max limitations of the lower and upper zone. This will prove that the water which needs to be updated in the simulation is higher than the maximum limitations of the layers.

Because of the persistent problem of the maximum limitation it is not

clear if the change in the state vector applied in this section had positive or negative effect in the assimilation. It is clear although, that the new state vector works; and so the stores are updated individually, but there is no proof that it improves the model.

CHAPTER 7

ENSEMBLE MOVING BATCH SMOOTHER

In the following sections, it is explained, how the Ensemble Moving Batch Smoother is applied. Firstly the functionality of the EnMB is analyzed and also the implementation steps are given. Finally the results and the discussion about them.

7.1 Ensemble Moving Batch Smoother

7.1.1 Implementation

The decision to use the Ensemble Moving Batch Smoother to assimilate data was taken in order to check if it is possible to use what is 'known' from the model about how the terrestrial water storage varies during the month, rather than using the interpolated data. So, the monthly GRACE data could be directly be used.

The Ensemble moving Batch which was used in this master thesis has length of batch window of 30 days. The use of it, is shown in the flow diagram in Figure 7.1. In the first part the forward model runs through the end of the smoother window to obtain the prior estimate of the state (as shown in Figure 7.2). An augmented state vector Y is created, which contains the states of the 5th, 15th and 25th day of the month (every ten days).

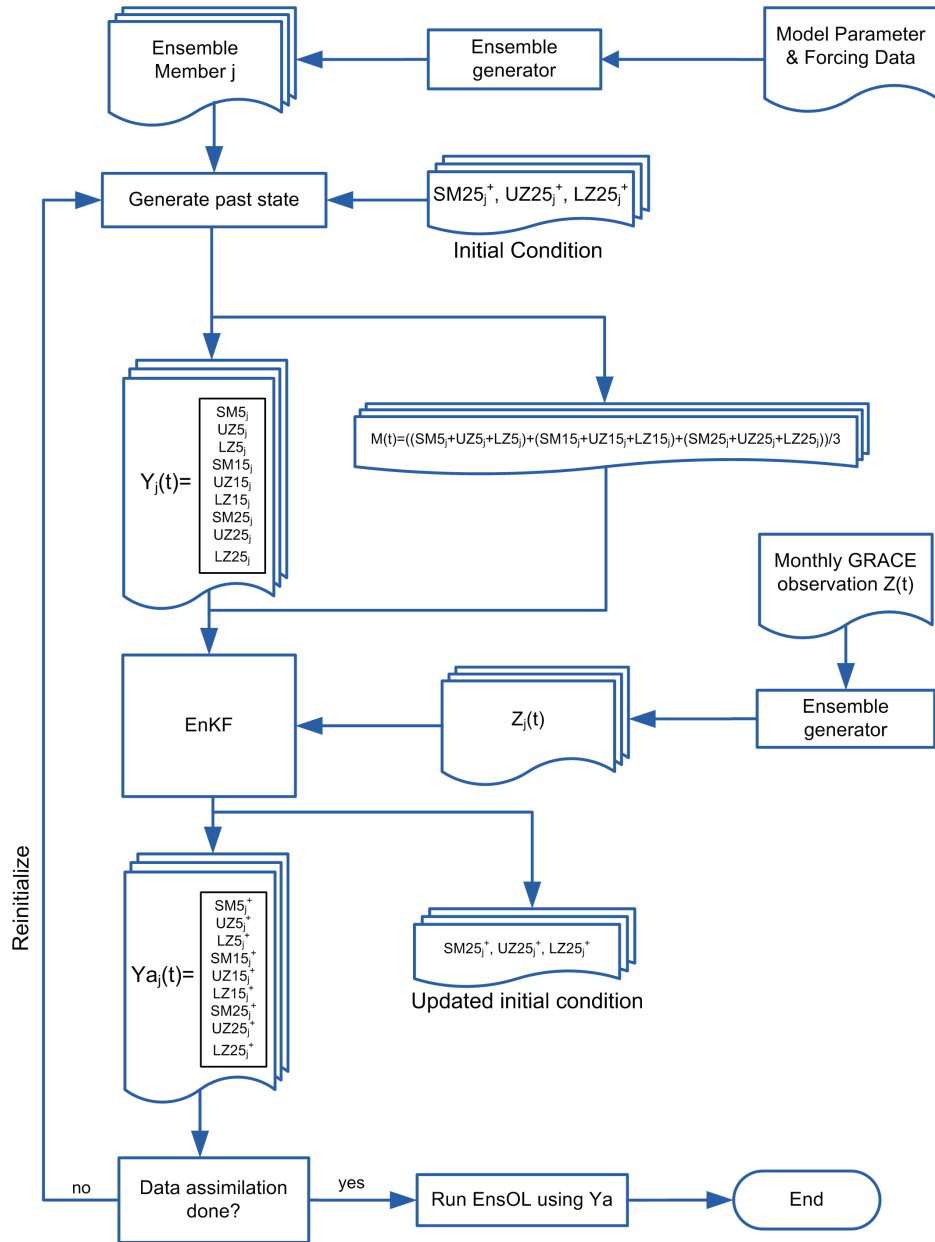


Figure 7.1: Flow diagram of the Ensemble Moving Batch Smoother

$$Y_j(t) = [SM_{j,5} \ UZ_{j,5} \ LZ_{j,5} \ SM_{j,15} \ UZ_{j,15} \ LZ_{j,15} \ SM_{j,25} \ UZ_{j,25} \ LZ_{j,25}]^T \quad (7.1)$$

where SM is soil moisture, UZ is the upper zone and LZ is the lower zone. As observation the GRACE DMT dataset was used. So the augmented

measurement vector Z contains each time the monthly value of GRACE observation. Then, the EnKF equations (as presented in previous sections) are applied to these augmented vectors to yield an updated estimate.

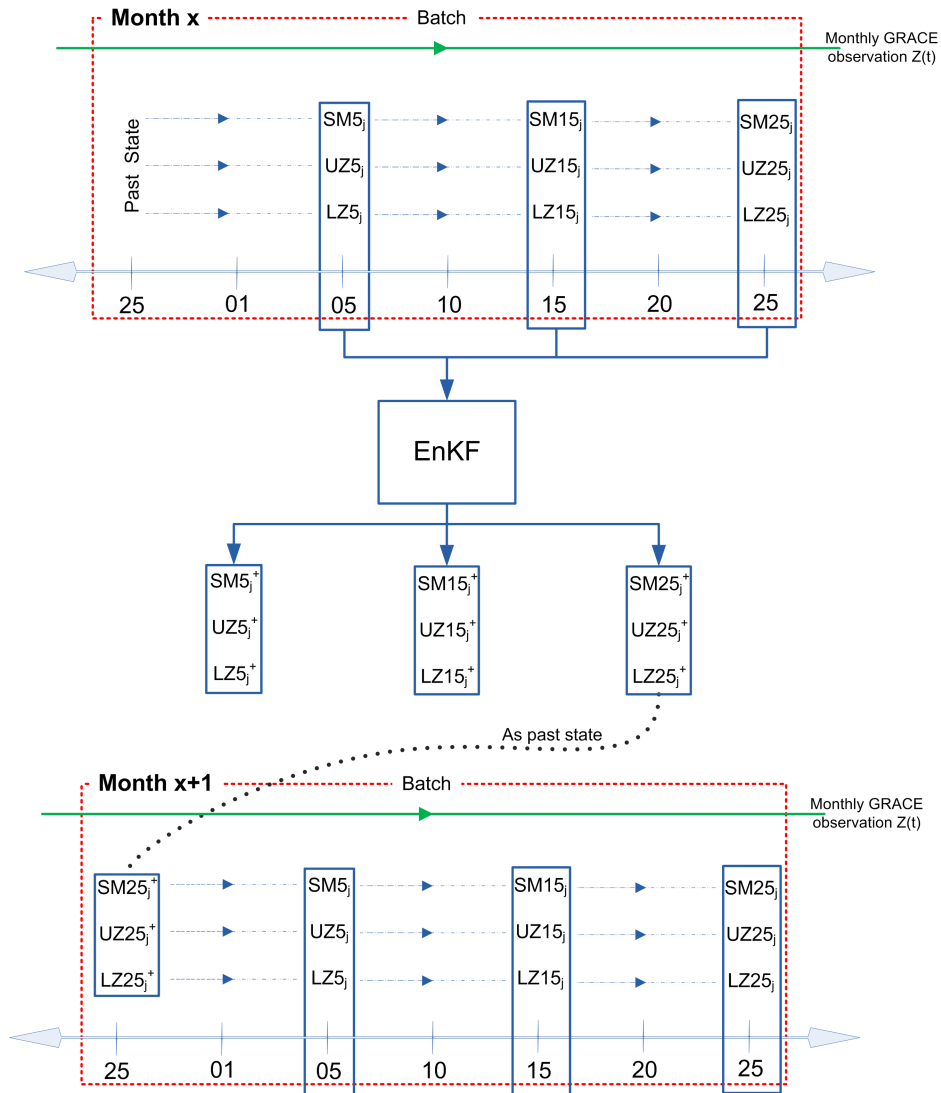


Figure 7.2: Conceptual diagram of the Ensemble Moving Batch Smoother used in this master thesis

From the update estimate created the SM_{j25}^+ , UZ_{j25}^+ , LZ_{j25}^+ are used as initial conditions for the first day of the batch for the next period, to run the forward model .

In Figure 7.2, the conceptual diagram of the EnMB used in this case is given. In the upper side of the figure forward model run for a *month x* is

shown. The batch window is shown with red color and the GRACE observation with the green line. After applying EnKF to the vector, the updated state vector $Ya(t)$ is produced. Then, as explained, the SM_j25^+ , UZ_j25^+ , LZ_j25^+ are used as prior state for the next month. For the first model run data from the Ensemble Open Loop were used as prior data.

Finally as shown in Figure 7.1 when the whole time span is covered, an Ensemble Open Loop is applied, using all the updated estimates $Ya(t)$, to get values for the in between days of the updates.

7.1.2 Results - Discussion

In this section the results of the Ensemble Moving Batch simulation are presented. In Figure 7.3 the mean of the averaged catchment is presented and at the same time is compared with the resulted mean of the averaged catchment of the Ensemble open loop.

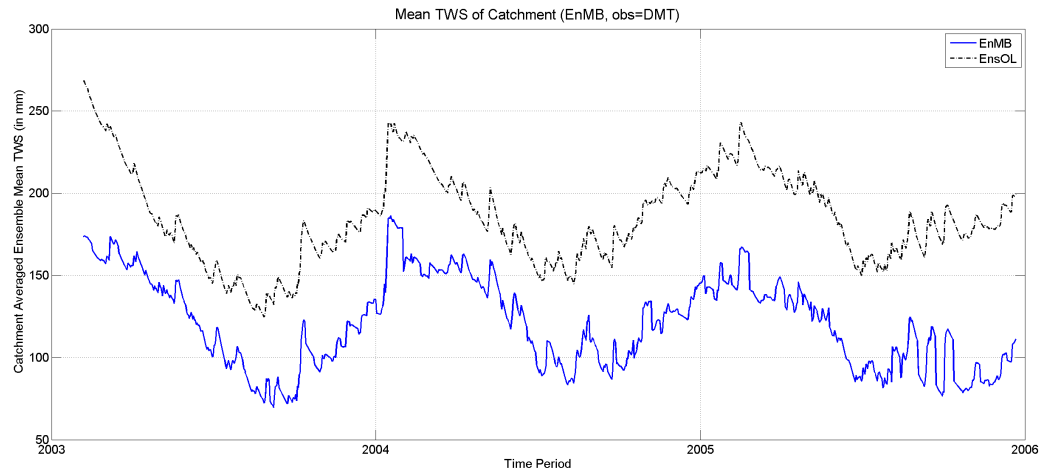


Figure 7.3: *Ensemble mean TWS of the averaged catchment for Ensemble Moving Batch and Ensemble Open Loop (DMT algorithm was used)*

Like in the previous chapter, when the state vector consisted of the different layers and when the maximum limitations were applied correctly, the mean values significantly lower compared with the Ensemble Open Loop. The annual pattern is followed also in this case and the new result is more smooth than the previous as expected after applying the Ensemble Moving Batch.

In Figure 7.4 the catchment averaged standard deviation of the TWS, from the Ensemble Moving Batch Smoother is given and it is compared with

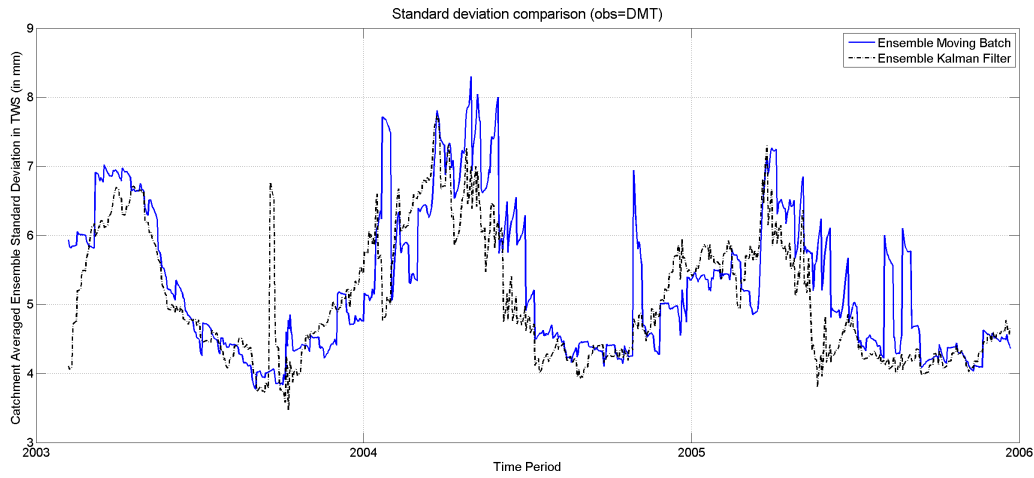


Figure 7.4: Averaged catchment ensemble standard deviation of TWS for the Ensemble Moving Batch and the Ensemble Kalman Filter (DMT algorithm was used)

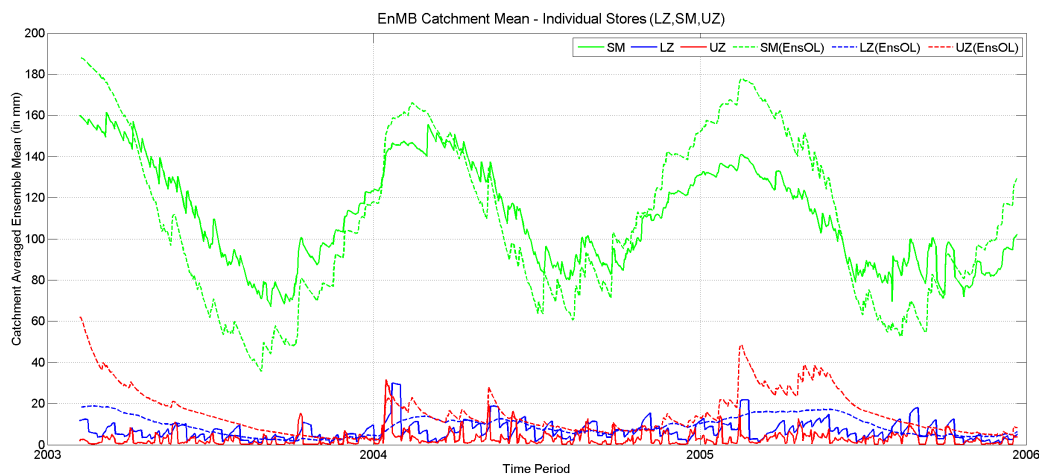


Figure 7.5: Comparison of individual stores for the Ensemble Moving Batch compared with the Ensemble Open Loop. SM is for soil moisture, UZ is for upper zone and LZ is for lower zone.

the Ensemble Kalman Filter simulation of the previous chapter (lower part of Figure 6.6), where the state vector includes the individual layers. The standard deviation values have the same phase, except of some spikes that both of the simulations have. The standard deviation values are really low if they are compared with the critical GRACE accuracy of $20mm$.

Observing Figures 7.3 and 7.4, the application of Ensemble Moving Batch

to the experiment can be characterized as successful. The annual pattern which is followed in Figure 7.3 and the low standard deviation in Figure 7.4 is the proof of that. The lower values of the mean TWS is an indication of the persistent problem with the maximum limitation of the lower and upper zone.

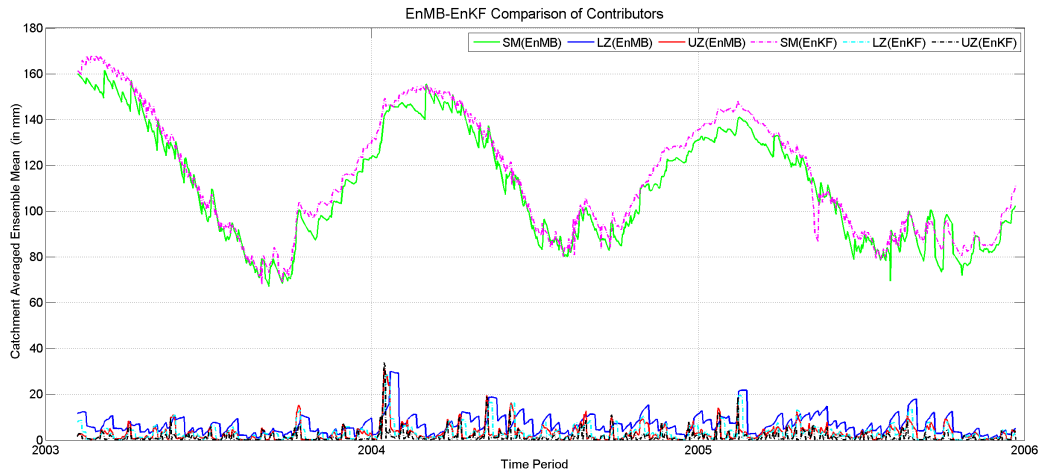


Figure 7.6: Individual stores for the Ensemble Moving Batch compared with the Ensemble Kalman Filter. SM is for soil moisture, UZ is for upper zone and LZ is for lower zone.

In Figure 7.5 the contributors of the Ensemble Moving Batch are shown and compared with the EnsOL. The behavior of the different layers in Ensemble moving batch are the same as the Ensemble Kalman Filter as shown in Figure 7.6 where they are compared. The lower and upper zone layers have low values compared to the EnsOL, but only lower zone is significantly lower than the EnsOL. Also here it is proved that the EnMB is working well and as expected, but the problem with the maximum limitations still remains.

Finally, in Figure 7.7 the soil moisture layer of the Ensemble moving batch is compared with EnsOL. As explained also earlier, their phase is similar; although the soil moisture of the EnsOL has bigger variations from the rain to the dry season.

In this figure is also shown the soil moisture of the Ensemble Moving Batch before the final step is done. This final step, as shown in the flow diagram of Figure 7.1, is the application of the EnsOL to create data for the days between the updates. It seems that in general the before the application of the EnsOL to the updates, they are quite smooth with not big variation

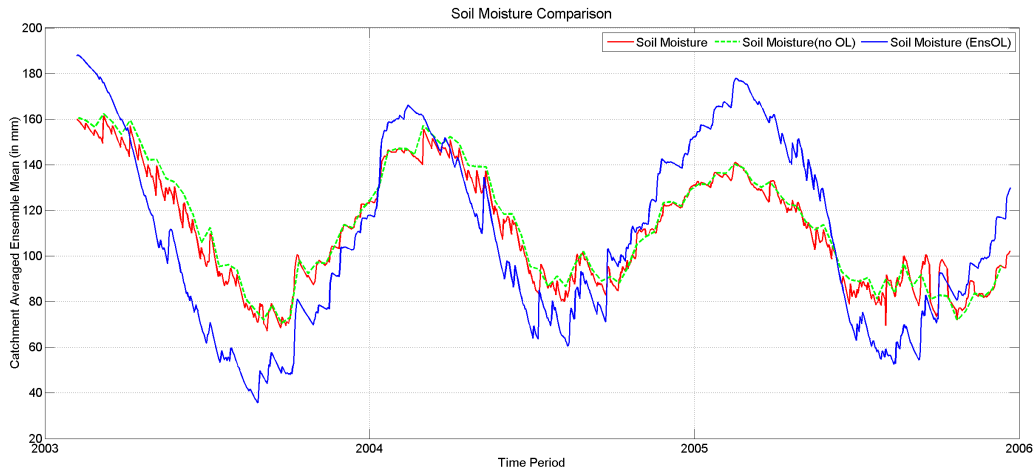


Figure 7.7: Comparison of the Soil Moisture layer for the Ensemble Moving Batch with the Ensemble Open Loop. The Ensemble Moving Batch is plotted with and without the final step of the EnsOL (in mm)

between them. Also, it is obvious that through the days that the EnsOL is applied the data are moving towards the Ensemble Open Loop simulation.

The experiment could be characterized successful also for another reason. Just by using the observation itself and the prior knowledge of model, the result is satisfying. The lower values in Figure 7.3 are because of the maximum limitation problem, as proved in the previous chapter. Soil moisture is reacting as expected in the simulation, and this is an indication that the mean TWS results might be corrected, if the maximum limitation problem is going to be solved.

7.2 EnMB with increased maximum limitations

7.2.1 Introduction

In previous sections it was mentioned several times that the maximum limitation of the lower and upper zone layers, it seems not to react as expected. In this section the limitations of the those two layers are slightly changed to become more flexible and to track the differences of the simulation.

7.2.2 Implementation

The Ensemble Moving Batch was also used in this simulation which worked as expected in the previous section. The GRACE observation was again the one created with the DMT algorithm, so as the results could be comparable with the previous ones.

The change which was applied in this simulation was to increase the allowed capacity in each layer. In this way it would be possible to check what is the amount of water which should be added by the update of the Ensemble Moving Batch and it is not allowed by the maximum limitations.

For both lower and upper zone the maximum limitation was set to 130% of the previous value of each one of them. So, in each update the limitations were:

- The same limitation for the soil moisture, which is the field capacity
- $LZ_{max} = 1.3 * LZ_{old}$ where the LZ_{old} is the old value of the Lower Zone and LZ_{max} is the maximum value of it
- $UZ_{max} = 1.3 * UZ_{old}$ where the UZ_{old} is the old value of the Upper Zone and UZ_{max} is the maximum value of it

In this simulation the final step of the EnMB (the EnsOL to create data for the days between the updates) was not applied, because this is a test for the maximum limitations of the lower and upper zone in the assimilation and not from the model. In every figure the updates of the Ensemble Moving Batch are denoted with a symbol and simply connected between them.

7.2.3 Results - Discussion

In Figure 7.8 the resultant mean value of the averaged catchment are plotted and compared with the simulation of the previous section of the chapter. At the same time the Ensemble Open Loop is plotted as well as the GRACE observation. The increase of the lower and upper zone capacity has allowed the terrestrial water storage capacity to increase. The phase of the stored water value through the whole time-span for both of the EnMB simulation is almost identical, but the increased limitation simulation has increased the TWS by 10 – 50 *mm* of water.

Except from the initial period of the experiment, the simulation seems to be closer to the GRACE simulation than the ensemble open loop, for the

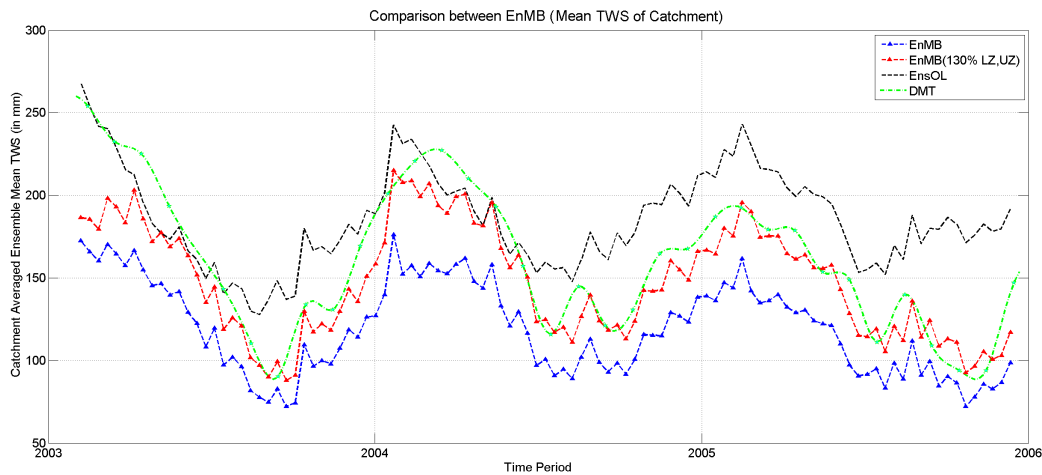


Figure 7.8: Averaged catchment ensemble mean TWS value for the Ensemble Moving Batch simulations, Ensemble Open Loop and GRACE observation. The different EnMB plots represent the old and new limitations of the Lower and Upper zone (in mm).

rest of the time span of the simulation, but at the same time to follow the pattern of the ensemble open loop.

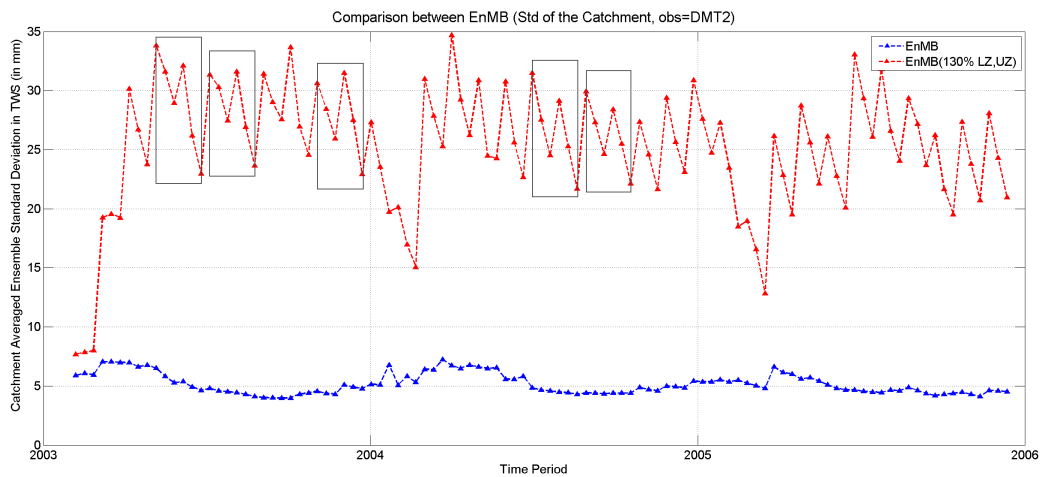


Figure 7.9: Averaged catchment ensemble standard deviation of the TWS for the Ensemble Moving Batch simulations. The different EnMB plots represent the old and new limitations of the Lower and Upper zone (in mm). The framed parts depict the 'M' pattern.

The standard deviation is plotted in Figure 7.9 and compared with the previous simulation. Increasing the lower and upper zone layer capacity had

the effect of increased standard deviation for the whole time span except for the initial period. The high values should be expected as the different ensemble members of the simulation have more flexibility to add water in those two layers with the increased maximum limitations.

In this figure an annual pattern is also visible. In the dry season the standard deviation has the lowest values of the season with almost half of the magnitude compared to the rain season. The maximum limitations are not frequently used in dry season because of water absence to fill in the layers and so the different ensemble members have more similar results.

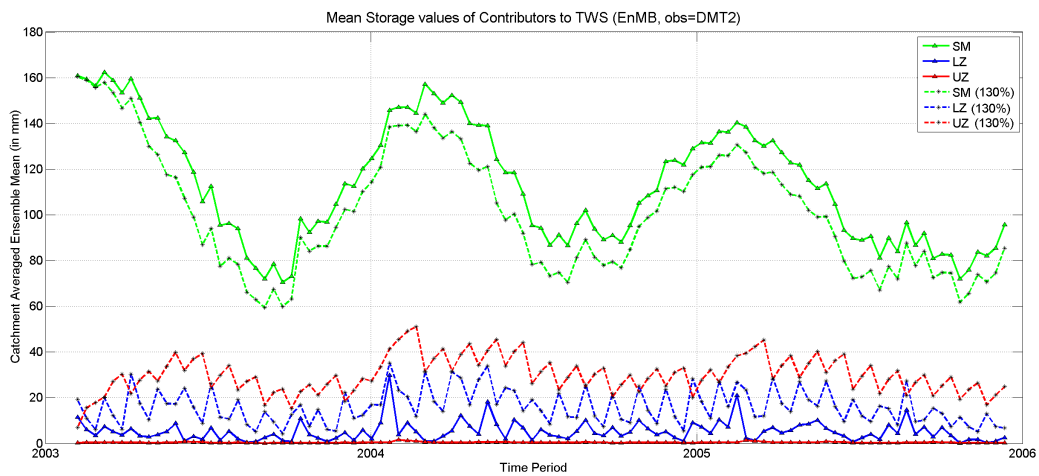


Figure 7.10: Individual stores for the different Ensemble Moving Batch simulations, with and without increased limitation for lower and upper zone. SM is for soil moisture, UZ is for upper zone and LZ is for lower zone (in mm)

Also, in Figure 7.9, there is an 'M' pattern repeated every 6 updates (as denoted with the frames in the figure). This could be because of the strange pattern followed by the upper and lower zone as shown in Figure 7.10. In this figure the individual storage terms are shown for the Ensemble Moving Batch with the old and revised limitations of upper zone and lower zone. The soil moisture of the increased limitation Ensemble moving batch is lower by 10 – 15 mm compared with the previous simulation. Upper zone layer appears to have slightly increased value with the increased maximum limitation, which was expected. But for the lower zone big difference revealed between the simulation with the different limitations. Before the change the lower zone had values close to zero but now it seems to have larger values even compared to the upper zone.

As mentioned in previous paragraph, the repeated 'M' pattern which appeared in Figure 7.9, could be explained by the strange pattern followed

by the upper and lower zone. Through the whole time span there is a repeated up and down movement for both of them but it appears in different direction. Also, the peaks in lower and upper zone in the limited and unlimited case occur at the same time.

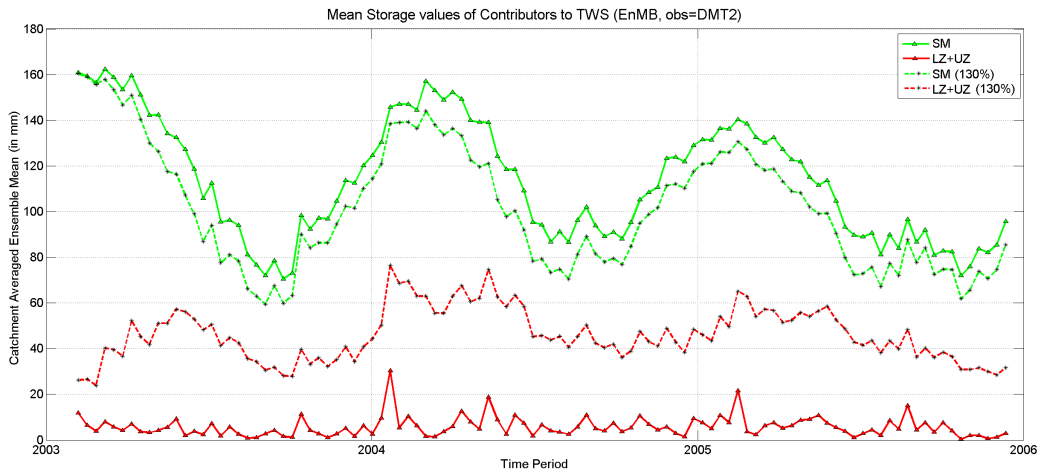


Figure 7.11: Individual stores for the different Ensemble Moving Batch simulations, with and without increased limitation for lower and upper zone. SM is for soil moisture, UZ+LZ is the accumulated lower and upper zone (in mm)

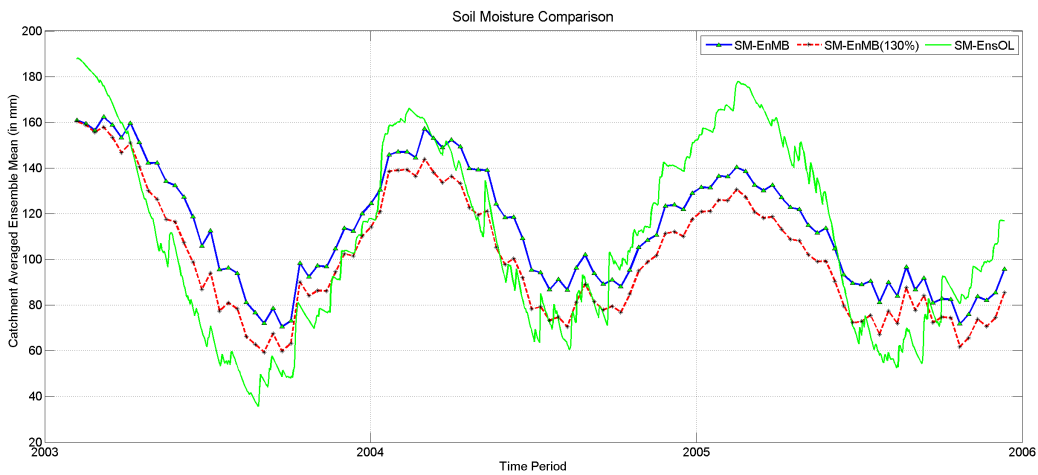


Figure 7.12: Comparison of the Soil Moisture layer for the Ensemble Moving Batch with the Ensemble Open Loop. The Ensemble Moving Batch is plotted with and without the final step of the EnsOL (in mm)

Because of repeated pattern of the lower and upper zone, Figure 7.11 was created. In this Figure the lower and upper zones are added together to

produce the ' $LZ + UZ$ ' layer. The new layer created looks like a nice slowly-varying storage term for both of the simulations. Both of the simulations seem to have the same attitude and changes through the whole time-span for this new layer. Also, there is not an annual pattern followed by both of them, but there are high spikes at the rain seasons and lower values for the dry season.

Figure 7.12 compares the Soil Moisture layer between the two different Ensemble Moving Batch simulations with the Ensemble Open Loop. As mentioned in a previous paragraph, the soil moisture of the increased limitation Ensemble moving batch is lower by $10 - 15mm$ compared with the previous simulation. But compared with the Ensemble Open Loop this does not seem to be incorrect.

In this master thesis there were four basic question which should be answered. Firstly it should be answered the question what leads to an update and if the seasonality is created by the winter or if the initial conditions create the ensemble spread. The next question which should be answered was to understand which one, of the given GRACE observations algorithms, provides better improvement to the model. The third research objective was to test Ensemble Moving Batch Smoother for data assimilation, in order to understand if using observations beyond the estimation time, could provide better results. Finally, the fourth research objective was to test a new state vector, where the individual stores of the Terrestrial Water Storage will be updated individually.

The first question was answered in section 5.1, where the simulation was done for an extended period. The period extension was the best way to check the seasonality and as expected, the new simulation with the three year time span proved that there is an annual pattern followed by the resulted terrestrial water storage values, with high values in the rainy season and low values for the dry season. The initial conditions are creating the high values observed in the very first steps of the simulation but this is corrected in the start of the second year and even more in the third year. The 'sawtooth' pattern and the ensemble spread was created from the bug found and corrected in the simulation code in section 5.2. After de-bugging, standard deviation had low values and the ensemble mean TWS of the averaged catchment didn't have the 'sawtooth' pattern any more.

The de-bugging result could be comparable with the Ensemble Open Loop

TWS or with the GRACE observation. This could provide answers for the different GRACE observation provided. This led to the next question on which different GRACE data sets were used in data assimilating, to understand which one provides better improvement to the model. Although that the results are more clear now (compared to Widiastuti (2009)), yet again it is not easy to conclude in which of the provided algorithms is the one that reacts in the most appropriate way and if it is improving the model. The results shown different behavior through the simulation period and none of them could be considered as incorrect or inappropriate. The only comment which should be done is that the DMT and RBF data-sets are following more close patterns than the CSR algorithm. Further action on the different GRACE algorithm comparison could be to check this difference between the DMT and RBF compared to the CSR algorithm.

The third research objective was the application of the Ensemble Moving Batch to assimilate the GRACE terrestrial water storage change data into the HBV-96 model. The Ensemble Moving Batch Smoother experiment was characterized as successful. The followed annual pattern and the low standard deviation is a proof of that. But because of the maximum limitation problem (which is discussed below) the TWS was significantly low, but the soil moisture is reacting as expected. So, EnMB should be used in future work to assimilate data as it has the advantage of using directly the monthly GRACE observations.

In section 6.1 the need for a more rational sequence of the state vector split was tested. The results were almost the same as previously and this was not what expected. The problem was traced on the maximum limitation of the lower zone and its application in the simulation. This problem was partly solved when the fourth research objective was implemented, which included the change of the state vector. The individual stores were added to it, with different use of the maximum limitation. When the soil moisture result was compared with the Ensemble Open Loop it was clear that it reacts more correctly and not just filled up until the maximum limitation was reached. But, at the same time, the lower values of the lower and upper zone was reducing the ensemble mean TWS of the averaged catchment value.

After the first application of the Ensemble Moving Batch, another test was done to explore even more in depth the maximum limitation problem of the lower zone. A change on the limitation was applied in the lower zone but also in the upper zone, in order to explore which could be the effect also on it. As a result the lower zone was increased significantly and upper zone was also increased, but not with the same magnitude. Also, after this simulation the TWS values for the whole time span was increased. Because of those

results, it is recommended that in future work research should be done on which should be the maximum limitation for those two layers and how they should be applied.

In all the simulation after the state vector change (section 6.2), when the maximum limitations are reached for soil moisture and upper zone there was a surplus of water, especially during the rainy season, which it wasn't used. In future work it should be considered the possibility to add the surplus of water to the next layers ($SM_{surplus} \rightarrow LZ$ and $LZ_{surplus} \rightarrow UZ$).

During further research based on the HBV-model, a new routing model should be used, which is already created for the HBV-model (Weerts, 2010). Better water distribution could produce more efficient result either in simple HBV-model simulations or in data assimilation simulations.

The correction of the leakage error could be the most interesting 'next step' in the research on this field. Leakage error is the effect of neighboring basins, when there is a 'leakage' of the signal from the neighboring area. This happens because GRACE is affected by such a large areas, especially when a spatial filter is applied to reduce the noise due to hydrological signals that vary with a timescale shorter than one month. Although the filter reduces these errors, it introduces new errors because part of the gravity anomaly of the target area leaks out of the target area and part of the outside anomaly leaks into the target area (For more details the leakage error is described by, e.g., Wahr et al. (1998), Swenson and Wahr (2002), Swenson et al. (2003), Winsemius et al. (2006)).

Research could be done to include the GRACE ground track information. Based on Winsemius et al. (2006) the within-month ground track coverage of GRACE could be added to the experiments and this could lead to better spatial distribution of the assimilation updates. It would be interesting if combined with the research on the leakage error.

BIBLIOGRAPHY

- S Bergstrom. Development and application of a conceptual runoff model for scandinavian catchments. *SMHI Report RHO*, 7:134, 1976.
- SV Bettadpur. Utcsrc level-2 processing standards document for level-2 product release 0004. *Center for Space Research, University of Texas at Austin*, 2007.
- F Bouttier and P Courtier. *ECMWF Data Assimilation Lecture notes*. ECMWF, 1999.
- DEOS. *DEOS Mass Transport model release 1 (DMT-1)*. Delft University of Technology, 2009.
- JCI Dooge. A general theory of the unit hydrograph. *Journal of Geophysics Res.*, 64(2):241–256, 1959.
- JP Drecourt. *Data assimilation in hydrological modelling [Report]*. PhD thesis, Technical University of Denmark, 2004.
- S. Dunne and D. Entekhabi. An ensemble-based reanalysis approach to land data assimilation. *Water Resour Res*, 41, 2005.
- S. Dunne and D. Entekhabi. Land surface state and flux estimation using the ensemble kalman smoother during the southern great plains 1997 field experiment. *Water Resour Res*, 42, 2006.
- en.wikipedia.org/wiki/Rhine.
- eosps0.gsfc.nasa.gov/. GRACE Brochure.

- G Evensen. Sequential data assimilation with a nonlinear quasi-geostrophic model using monte carlo methods to forecast error statistics. *Journal of Geophysical Research*, 99:10, 143–10, 162, 1994.
- G Evensen. The ensemble kalman filter: theoretical formulation and practical implementation. *Ocean Dynamics*, 53:343–367, 2003.
- G Evensen. *Data Assimilation*. Springer, 2007.
- G Evensen and PJ van Leeuwen. An ensemble kalman smoother for nonlinear dynamics. *Mon Weather*, 128:1852–1867, 2000.
- Dr. Brian C. Gunter. Personal communication, 2010.
- Christofer Jekeli. Alternative methods to smooth the earth’s gravity field. Geodetic and Geoinformation Science, Department of Civil and Env. Engineering and Geodetic Science, The Ohio State University, Report No.327 1981.
- R Klees, EA Zapreeva, HC Winsemius, and HHG Savenije. The bias in grace estimates of continental water storage variations. *Hydrology and Earth System Sciences Discussions*, 3:3557–3594, 2006.
- R Klees, X Liu, T Wittwer, BC Gunter, EA Revtova, R Tenzer, P Ditmar, HC Winsemius, and HHG Savenije. A comparison of global and regional grace models for land hydrology. *Surv Geophys*, 29:335–359, 2008a.
- R Klees, E Revtova, BC Gunter, P Ditmar, E Oudman HC Winsemius, and HHG Savenije. The design of an optimal filter for monthly grace gravity models. *Geophysical Journal International*, 175:417–432, 2008b.
- J Kusche. Approximate decorrelation and non-isotropic smoothing of time-variable grace-type gravity field models. *Journal of Geodesy*, 81:733–749, 2007.
- G Lindstrom, B Johansson, M Persson, M Gardelin, and S Bergstrom. Development and test of the distributed hbv-96 hydrological model. *Journal of Hydrology*, 201:272–288, 1997.
- RK Linsley. The relation between rainfall and runoff. *Journal of Hydrology*, 5:297–311, 1967.
- X Liu. *Global gravity field recovery from satellite-to-satellite tracking data with the acceleration approach*. PhD thesis, TU Delft, 2008. URL <http://www.ncg.knaw.nl/>.

- X. Liu, P. Ditmar, C. Siemes, D.C. Slobbe, E. Revtova, R. Klees, R. Riva, and Q. Zhao. Deos mass transport model (dmt-1) based on grace satellite data: methodology and validation. *Geophysical Journal International*, 181:769788, 2010.
- H Madsen and R Canizares. Comparison of extended and ensemble kalman fitlers for data assimilation in coastal area modelling. *International Journal For Numerical Methods in Fluids*, 31:961–981, 1999.
- S. A. Margulis, D. McLaughlin, D. Entekhabi, and S. Dunne. Land data assimilation and estimation of soil moisture using measurements from the southern great plains 1997 field experiment. *Water Resour Res*, 38, 2002.
- JE Nash. A unit hydrograph study, with particular reference to british catchments. *Proc. Inst. Civ. Eng.*, 17:249–282, 1960.
- G Ramillien, A Cazenave, and O Brunau. Global time variations of hydrological signals from grace satellite gravimetry. *Geophys Journal*, 158:813826, 2004.
- G Ramillien, JS Famiglietti, and J Wahr. Detection of continental hydrology and glaciology signals from grace: A review. *Surv Geophys*, 29:361–374, 2008.
- Rolf H. Reichle, Dennis B. Mclaughlin, and Dara Entekhabi. Hydrologic data assimilation with the ensemble kalman filter, 2002.
- M Rodell and J Famiglietti. Detectability of variations in continental water storage from satellite observations of the time dependent gravity field. *Water Resour Res*, 35:27052723, 1999.
- M Rodell and J Famiglietti. An analysis of terrestrial water storage variations in illinois with implications for the gravity recovery and climate experiment (grace). *Water Resour Res*, 37:13271339, 2001.
- M Rodell and JS Famiglietti. The potential for satellite-based monitoring of groundwater storage changes using grace: the high plains aquifer, central us. *Journal of Hydrology*, 263:245–256, 2002.
- M Rodell, J Chen, H Kato, JS Famiglietti, J Nigro, and CR Wilson. Estimating groundwater storage changes in the mississippi river basin (usa) using grace. *Hydrogeology Journal of Geophysical Resaerch*, 15:159–166, 2007.

- R Schmidt, P Schwintzer, F Flechtner, C Reigber, A Guntner, P Doll, G Ramillien, A Cazenave, S Petrovic, H Jochmann, and J Wunsch. Grace observations of changes in continental water storage. *Global and Planetary Change*, 50:112–126, 2006.
- R Schmidt, F Flechtner, U Meyer, KH Neumayer, C Dahle, R Konig, and J Kusche. Hydrological signals observed by the grace satellites. *Surv Geophys*, 29:319–334, 2008.
- J Seibert. *Conceptual runoff models - fiction or representation of reality? Acta Univ. Ups., Comprehensive Summaries of Uppsala Dissertations from the Faculty of Science and Technology 436. 52 pp. Uppsala. ISBN 91-554-4402-4.* PhD thesis, Acta Univ. Upsala, 1999.
- EM Shaw. *Hydrology in Practise.* VNR International, 1983.
- S. Swenson and J. Wahr. Methods for inferring regional surface- mass anomalies from gravity recovery and climate experiment (grace) measurements of time-variable gravity. *J. Geophys. Res.*, 107, 2002.
- S Swenson and J Wahr. Post-processing of correlated errors in grace data. *Geophys Res Lett*, 33, 2006.
- S. Swenson, J. Wahr, and P. C. D. Milly. Estimated accuracies of regional water storage variations inferred from the gravity recovery and climate experiment (grace). *Water Resour. Res.*, 39, 2003.
- S. Swenson, D. Chambers, and J. Wahr. Estimating geocenter variations from a combination of grace and ocean model output. *J. Geophys. Res.*, 113, 2008.
- TH Syed, JS Famiglietti, M Rodell, J Chen, and CR Wilson. Analysis of terrestrial water storage changes from grace and gldas. *Water Resources Research*, 44, 2008.
- BD Tapley, S Bettapur, JC Ries, PF Thomson, and M Watkins. Grace measurements of mass variability in the earth system. *Science*, 305:503–505, 2004.
- W Terink, RTWL Hurkmans, PJJF Torfs, and R Uijlenhoet. Evaluation of a bias correction method applied to downscaled precipitation and temperature reanalysis data for the rhine basin. *Hydrol. Earth Syst. Sci.*, 14, 687703, 2010, 14:687–703, 2010.

- J. Wahr, M. Molenaar, and F. Bryan. Time variability of the earth's gravity field: Hydrological and oceanic effects and their possible detection using grace. , *J. Geophys. Res.*, 103:30205–30229, 1998.
- J Wahr, S Swenson, V Zlotnicki, and I Velicogna. Time-variable gravity from grace: first results. *Geophys Res Lett*, 31, 2004.
- AH Weerts, D Meiner, and S Rademacher. *Input data rainfall-runoff model operational systems FEWS-NL & FEWS-DE*. Deltares, 2008.
- Dr. Albrecht Weerts. Personal communication, 2010.
- S Werth, A Guntner, S Petrovic, and R Schmidt. Integration of grace mass variations into a global hydrological model. *Earth and Planetary Science Letters*, 277:166–173, 2009.
- E Widiastuti. Data assimilation of grace terrestrial water storage data into a hydrological model using the ensemble kalman smoother. Master's thesis, TUDelft, 2009.
- HC Winsemius, HHG Savenije, NC van de Giesen, BJJM van den Hurk, EA Zapreeva, and R Klees. Assessment of gravity recovery and climate experiment (grace) temporal signature over the upper zambezi. *Water Resources Research*, 42, 2006.
- T Wittwer. *Regional gravity field modelling with radial basis functions*. PhD thesis, NCG, Netherlands Geodetic Commission, 2009.
- M Wolff. Direct measurements of the earth's gravitational potential using a satellite pair. *Journal of Geophysical Research*, 74:5295–5300, 1969.
- www.etymonline.com/.
- www.grid.unep.ch.
- www.nasa.gov.
- www.smhi.se/en.
- www.unesco ihe.org/.
- www.usgcrp.gov/.
- www.waterandclimate.org/.

